4-30-2023

Brownian Dynamics Simulations of Interacting Magnetic Tri-axial Ellipsoids

Daniel Holmes Duke

Brownian Dynamics Simulations of Interacting Magnetic Tri-axial Ellipsoids

by

Daniel Holmes Duke

An Honors Capstone

submitted in partial fulfillment of the requirements

for the Honors Diploma

to

The Honors College

of

The University of Alabama in Huntsville

April 30, 2023

Honors Capstone Director: Dr. Isaac Torres-Diaz

Assistant Professor of Chemical Engineering

DocuSigned by:
Daniel Duke
1848D0D5EDC6423...
Student (signature) 4/30/2023 Date

DocuSigned by:
3A1301902138448...
Director (signature) 4/30/2023 Date

DocuSigned by:
Yu Lei
32CA807E51DF4EA...
Department Chair (signature) 4/30/2023 Date

William Wilkerson Digitally signed by William Wilkerson
Date: 2023.05.02 11:58:16 -05'00'
Honors College Dean (signature) Date

HONORS COLLEGE
THE UNIVERSITY OF ALABAMA IN HUNTSVILLE

Honors College
Frank Franz Hall
+1 (256) 824-6450 (voice)
+1 (256) 824-7339 (fax)
honors@uah.edu

Honors Thesis Copyright Permission

This form must be signed by the student and submitted as a bound part of the thesis.

In presenting this thesis in partial fulfillment of the requirements for Honors Diploma or Certificate from The University of Alabama in Huntsville, I agree that the Library of this University shall make it freely available for inspection. I further agree that permission for extensive copying for scholarly purposes may be granted by my advisor or, in his/her absence, by the Chair of the Department, Director of the Program, or the Dean of the Honors College. It is also understood that due recognition shall be given to me and to The University of Alabama in Huntsville in any scholarly use which may be made of any material in this thesis.

Daniel Duke

Student Name (printed)

DocuSigned by:
Daniel Duke
1848D0D5EDC6423...

Student Signature

4/30/2023

Date

Contents

Abstract

Magnetic nanorobots have immense potential for medical treatment at the cellular level. Colloidal nanorobots with independent locomotion and multi-actuating capabilities controlled by electromagnetic fields are still challenging. Our approach to fabricate nanorobots uses the dipolar interaction between anisotropic particles with different shapes and materials to generate tunable configurations between particles. Quantifying the high-dimensional dependence of dipolar interactions of tri-axial particles in position and orientation is crucial to model magnetic nanorobots. We report the analytical expressions for the interaction dipolar forces and torques between permanently magnetized tri-axial ellipsoids with different shapes and materials. We combine the novel ellipsoid-dipole model with unit quaternions to parameterize the orientational space. The analytical expressions capture the established behavior of uniform magnetic spheres. Additionally, we report Brownian dynamics simulations of interacting permanently magnetized ellipsoids under the influence of time-varying magnetic fields. We will show simulation results for binary systems composed of tri-axial ellipsoids with different shapes and sizes. We characterize the relative dynamic patterns between particles in the relative particle space. Simulation results show a synchronous particle rotation for small dipolar interactions; however, results show coupling rotation dynamics for strong dipolar interactions.

Chapter 1

Introduction

The term "nanorobot" aptly describes its own meaning: nano-sized robots. More specifically, nanorobots are externally controllable nano-sized structures on the that can operate and perform tasks on the nano-scale. In recent years, nanorobots have stimulated considerable excitement due their potential applications in a variety of fields, particularly in medicine. Several possible applications include cancer treatment, precise dental surgery, magnetic and ultrasound imaging, minimally invasive brain surgery, blood monitoring, and targeted drug delivery [1]. Current designs for nanorobots span a wide array of functionalities and capabilities, but at the most basic level all nanobots have two critical capabilities: they must convert external forms of energy into locomotion, and their direction of movement must be externally controllable. However, constructing nanorobots even with just these two capabilities has proven difficult. In general, as the the scale of the fabrication process decreases, robots lose functionality and tunability. Currently, the challenge of fabricating controllable nanorobots has not been overcome.

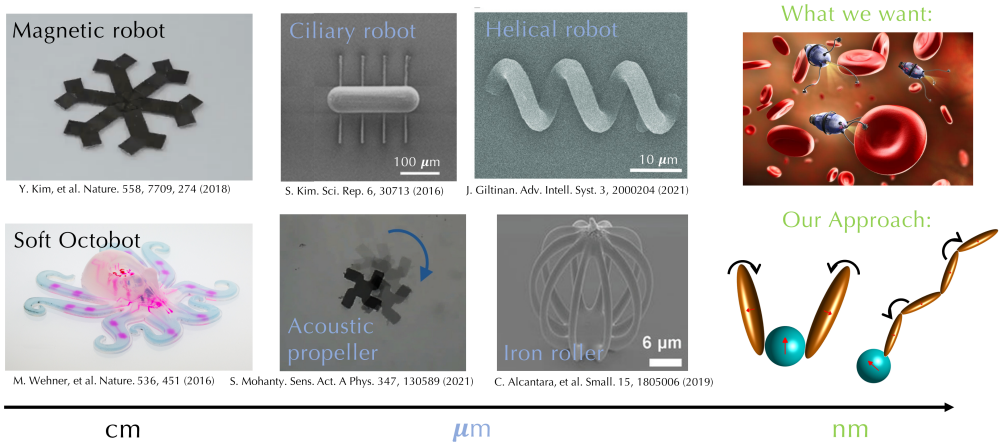

Figure 1.1: Examples from current literature of multi-actuation robots on the centimeter and micrometer scale [2] [3] [4] [5] [6] [7].

To solve this problem, we propose using combinations of magnetized ellipsoidal nanoparticles with various shapes, materials, and magnetizations, as illustrated in Figure 1.1. This design has several unique advantages. First, the simple shapes involved in the design make fabrication significantly more simple and feasible than other, more complex structures. Second, the shape anisotropy of the particles permits them to overcome the Scallop Theorem, which states that locomotion in low Reynolds numbers requires some asymmetry of motion [11]. Third, the magnetization of the particles affords a simple method for giving them energy and controlling their direction of movement. Finally, the immense design space formed through choice of particle material, shape, size, and magnetization offers a diverse range of possibilities when searching combinations of particles to form the most effective nanorobots for specific purposes.

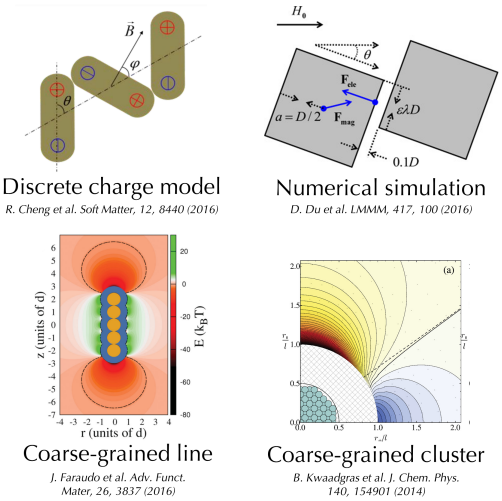

Figure 1.2: Current models for quantifying dipolar interaction of anisotropic colloids [8] [9] [9] [10].

In order to efficiently and thoroughly explore this design space and inform the construction of the first nanorobots, interaction dynamics of ellipsoidal nanoparticles must first be modeled and simulated. However, no analytical method currently exist for modeling the dipolar interaction of ellipsoids (Figure 1.2), a vital component of the interaction of two magnetized particles in close proximity. This report aims to tackles this challenge. To be specific, this report proposes a novel analytical model, termed the ellipsoid-dipole model, for the magnetic dynamics between two tri-axial ellipsoids and tests this model through both numerical calculations and comparisons with the established point-dipole model. Then, the report applies this model using Brownian dynamics simulations with a time-varying magnetic field to analyze the overall effect of dipolar interaction on particle dynamics in various conditions. First and foremost, the following two sections give some mathematical standards and background useful for clarifying the subsequent pages.

1.1 Dimensionless Variables

In order to easily extend the results of this work to various types of particles in various environments, all time and length measurements are made dimensionless. For a given time t and length l, equations (1.1.1) and (1.1.2) give the corresponding dimensionless forms $\widetilde{t}$ and $\widetilde{l}$, respectively:

$$\widetilde{t} = tD_{r,max}, \tag{1.1.1}$$

$$\widetilde{l} = \frac{l}{r_m}, \tag{1.1.2}$$

where $D_{r,max}$ is largest diagonal component of the rotational diffusivity tensor $\mathbf{D}_r$ of the particle, and r_m is the minimum particle semi-axis. When simulating multiple particles, the diffusivity tensors of all the particles must be compared to find the universally largest term. In addition to time and length, all force and torque variables are made dimensionless through comparison with Brownian energy. Equation (1.1.3) defines the relationship between a given energy U and its dimensionless form $\widetilde{U}$:

$$\widetilde{U} = \frac{U}{k_B T}, \tag{1.1.3}$$

where k_B is the Boltzmann constant and T is absolute temperature. Given this relation, equations (1.1.4) and (1.1.5) give the dimensionless forms of a given force F and torque τ:

$$\widetilde{F} = \frac{r_m}{k_B T} F, \tag{1.1.4}$$

$$\widetilde{\tau} = \frac{\tau}{k_B T}. \tag{1.1.5}$$

Over the course of this report, several dimensionless parameters are defined that describe the relative strengths of various interactions with respect to Brownian motion. Namely, β describes the strength of dipole-dipole interactions; α characterizes the strength of dipole-field interactions, and Z defines the strength of the electrostatic repulsion. Defining these parameters simplifies the process of quantifying and evaluating how the particles interact under varied conditions.

1.2 Spatial Representations

When modeling the interactions of more than one particle, defining relative positions and orientations of particles becomes key. First, a laboratory coordinate system, in which vectors define the position of particles in each coordinate direction, is established. The relative position of the particles in lab coordinates is found by subtracting the position vector of one particle from the position vector of the other. Ellipsoidal coordinates prove useful when characterizing the relative position of particles. Consider a particle with a coordinate system attached to its principal semi-axes. The ellipsoidal coordinate ξ at a relative position (x, y, z) measured in the particle coordinate system equals the real root of

$$\frac{x^2}{r_x^2 + \xi} + \frac{y^2}{r_y^2 + \xi} + \frac{z^2}{r_z^2 + \xi} = 1, \tag{1.2.1}$$

where r_x, r_y, and r_z are the principal semi-axes of the particle.

The orientation of the particles is described by the commonly used set of 3-1-3 Euler angles, denoted by θ, ϕ, and ψ. Respectively, these angles rotate counterclockwise around the z-axis, then the x-axis, then the z-axis.

Again, consider a particle with a coordinate system attached to its principal semi-axes. The orientation of this particle with respect to lab coordinates can be described by the Euler angles needed to rotate the lab coordinate system to the particle coordinate system. A transformation matrix that rotates a vector from lab space to particle space can be directly defined by these angles. However, in certain cases where the Euler angles align, a degree of freedom is lost and the orientation of the particle is not fully defined, a phenomenon known as Gimbal lock. Thus, the orientation of the particle is described using quaternions as expressed by

$$\mathbf{q} = q_0 + q_1\mathbf{i} + q_2\mathbf{j} + q_3\mathbf{k}. \tag{1.2.2}$$

To preserve the rigidity of the transformations, the quaternion elements are normalized according to

$$q_0^2 + q_1^2 + q_2^2 + q_3^2 = 1. \tag{1.2.3}$$

Based on Evans [12], the elements of the quaternion, known as the Euler-Rodrigues parameters, are defined from the Euler angles as

$$q_0 = cos\left(\frac{\phi}{2}\right) cos\left(\frac{\psi+\theta}{2}\right), \tag{1.2.4}$$

$$q_1 = -sin\left(\frac{\phi}{2}\right) cos\left(\frac{\psi-\theta}{2}\right), \tag{1.2.5}$$

$$q_2 = sin\left(\frac{\phi}{2}\right) sin\left(\frac{\psi-\theta}{2}\right), \tag{1.2.6}$$

$$q_3 = -cos\left(\frac{\phi}{2}\right) sin\left(\frac{\psi+\theta}{2}\right). \tag{1.2.7}$$

The Euler-Rodrigues parameters completely describe without singularities any relative orientation and are thus suitable to describe the orientation of particles. Consider a particle I an orientation relative to lab space described by a quaternion. Based on O'Reielly [13], The transformation matrix from lab space to particle I space in terms of the Euler-Rodrigues parameters equals

$$\mathbf{A} = \begin{bmatrix} q_0^2 + q_1^2 - q_2^2 - q_3^2 & 2(q_1q_2 - q_0q_3) & 2(q_1q_3 + q_0q_2) \\ 2(q_2q_1 + q_0q_3) & q_0^2 - q_1^2 + q_2^2 - q_3^2 & 2(q_2q_3 - q_0q_1) \\ 2(q_3q_1 - q_0q_2) & 2(q_3q_2 + q_0q_1) & q_0^2 - q_1^2 - q_2^2 + q_3^2 \end{bmatrix}. \tag{1.2.8}$$

Consider particle J with its own coordinate system, quaternion, and transformation matrix. The relative orientation between particle I and particle J can be described by a relative quaternion given by

$$\begin{bmatrix} q_0^{IJ} \\ q_1^{IJ} \\ q_2^{IJ} \\ q_3^{IJ} \end{bmatrix} = \begin{bmatrix} q_0^J & q_1^J & q_2^J & q_3^J \\ -q_1^J & q_0^J & -{q_3}^J & \xi^J \\ -q_2^J & q_3^J & q_0^J & -q_1^J \\ -q_3^J & -{q_2}^J & q_1^J & q_0^J \end{bmatrix} \cdot \begin{bmatrix} q_0^I \\ q_1^I \\ q_2^I \\ q_3^I \end{bmatrix}, \tag{1.2.9}$$

which can then be used in equation (1.2.8) to produce a transformation matrix from particle J space to particle I space.

Quaternions have several intriguing properties, many of which aid in maximizing the efficiency of calculations. For example, because normalized quaternions produce an orthogonal transformation matrix, the inverse of a transformation matrix, which rotates back to the original coordinate system, equals its transpose. Furthermore, relating quaternions to their corresponding transformation matrices requires only arithmetic, unlike the Euler angles, which require computationally expensive trigonometric calculations.

Chapter 2

Ellipsoid-Dipole Model

2.1 Interaction Energy

When two magnetized particles are close enough, the magnetic field of each particle will interact with the dipole of the other particle. The interaction of a dipole in a magnetic field will have a potential energy that depends on the magnitude and direction of the magnetic moments and the relative position and orientation of the particles. Consider two magnetized ellipsoids, particle I and particle J. The potential energy resulting from the particle J dipole interacting with the particle I field will have a magnitude described by

$$U^{IJ} = -\mathbf{m}^J \cdot \mathbf{H}^I, \tag{2.1.1}$$

where $\mathbf{m}^J$ is the magnetic moment of particle J and $\mathbf{H}^I$ is the magnetic field of particle I. Using the definition of magnetic moment ($\mathbf{m} = \mu_0 v_p \mathbf{M}$),

$$U^{IJ} = -\mu_0 v_p^J \mathbf{M}^J \cdot \mathbf{H}^I \tag{2.1.2}$$

gives another description of dipolar interaction energy, where v_p^J is the volume of particle J, μ_0 is the vacuum permeability, and $\mathbf{M}^J$ is the magnetization of particle J.

$$\mathbf{H}^I = \left(\frac{r_x^I r_y^I r_z^I}{2}\right) \mathbf{G}^I \cdot \mathbf{M}^I = \left(\frac{3v_p^I}{8\pi}\right) \mathbf{G}^I \cdot \mathbf{M}^I \tag{2.1.3}$$

gives the magnetic field of an ellipsoidal particle I, where r_x^I, r_y^I, and r_z^I are the principal semi-axes of particle I, $\mathbf{G}^I$ is the Green tensor for particle I evaluated at the relative position of particle J, v_p^I is the volume of particle I, and $\mathbf{M}^I$ is the magnetization of particle I. Substituting this into equation (2.1.2) and using the transformation matrix $\mathbf{A}^{JI}$ to transform from particle I space to particle J space yields

$$U^{IJ} = -\left(\frac{3\mu_0 v_p^J v_p^I}{8\pi}\right)\mathbf{M}^J \cdot \mathbf{A}^{JI} \cdot \mathbf{G}^I \cdot \mathbf{M}^I, \tag{2.1.4}$$

which can be further simplified by factoring out the magnitude of the magnetization vectors and applying the definition of magnetic moment, resulting in

$$U^{IJ} = -\left(\frac{3(\mu_0 v_p^J M^J)(\mu_0 v_p^I M^I)}{8\pi\mu_0}\right)\widetilde{\mathbf{M}}^J \cdot \mathbf{A}^{JI} \cdot \mathbf{G}^I \cdot \widetilde{\mathbf{M}}^I,$$

$$U^{IJ} = -\left(\frac{3m^J m^I}{8\pi\mu_0}\right)\widetilde{\mathbf{M}}^J \cdot \mathbf{A}^{JI} \cdot \mathbf{G}^I \cdot \widetilde{\mathbf{M}}^I, \tag{2.1.5}$$

where $\widetilde{\mathbf{M}}^J$ and $\widetilde{\mathbf{M}}^I$ are the unit vectors in the direction of the magnetizations of particles J and I, respectively, and m^J and m^I are the magnitudes of the magnetic moment of particles J and I, respectively.

The Green tensor characterizes the magnetic field of an ellipsoidal particle at a position defined by a relative position vector and the associated ellipsoidal coordinate ξ. Equation (2.1.6) gives the components of the Green tensor:

$$G_{ij} = \delta_{ij}\left(L_{r_j}(\xi) - L_{r_j}(\infty)\right) + x_j\frac{\delta L_{r_j}(\xi)}{\delta x_i}, \tag{2.1.6}$$

where δ_{ij} is the Kronecker delta and L_{r_j} is the shape parameter function defined by

$$L_{r_j}(\xi) = \int_0^{\xi} F_{r_j}(\alpha)\, d\alpha, \tag{2.1.7}$$

$$F_{r_j}(\alpha) = \frac{1}{(\alpha + r_j^2)\sqrt{(\alpha + r_x^2)(\alpha + r_y^2)(\alpha + r_z^2)}}. \tag{2.1.8}$$

To make the Green tensor dimensionless, the measurements of distance (particle semi-axes and relative position) are related to their dimensionless form in the manner described by equation (1.1.2):

$$\widetilde{x}_i = \frac{x_i}{r_m}, \quad \widetilde{r}_i = \frac{r_i}{r_m}. \tag{2.1.9}$$

From Appendix A, dimensionless analysis of the Green tensor using these identities yields

$$\mathbf{G}_{ij} = \frac{1}{r_m^3}\widetilde{\mathbf{G}}_{ij}, \tag{2.1.10}$$

where $\widetilde{\mathbf{G}}_{ij}$ is the dimensionless Green tensor as a function of $\widetilde{x}_i$ and $\widetilde{r}_i$. Using this identity in equation (2.1.5) and defining the dimensionless variable $\widetilde{U}^{IJ}$ according to equation (1.1.3) yields

$$\widetilde{U}^{IJ} = -\beta \cdot \widetilde{\mathbf{M}}^J \cdot \mathbf{A}^{JI} \cdot \widetilde{\mathbf{G}}^I \cdot \widetilde{\mathbf{M}}^I, \tag{2.1.11}$$

which describes the dimensionless dipolar interaction energy, where

$$\beta \equiv \frac{3m^J m^I}{8\pi\mu_0 r_m^3 k_B T}. \tag{2.1.12}$$

When comparing the interactions of particles with different shapes, it becomes useful to relate the dipolar interaction parameter β for each particle to the that of a sphere with radius r_m. To relate these two parameters,

$$v_p = \widetilde{r}_x \widetilde{r}_y \widetilde{r}_z v_s \tag{2.1.13}$$

is used to relate the volumes of a sphere and an ellipsoid with the same r_m. Applying this relationship to equation (2.1.12) results in

$$\beta_e = \left(\widetilde{r}_x^I \widetilde{r}_y^I \widetilde{r}_z^I\right)\left(\widetilde{r}_x^J \widetilde{r}_y^J \widetilde{r}_z^J\right)\beta_s, \tag{2.1.14}$$

where v_p is the volume of an ellipsoid and v_s is the volume of a sphere with a radius equal to r_m of the ellipsoid, and β_e and β_s are the associated dipolar interaction parameters.

To find the dipolar interaction energy of the entire system, the potential energy of the particle I dipole interacting with the particle J field must also be considered:

$$\widetilde{U}^{JI} = -\beta \cdot \widetilde{\mathbf{M}}^I \cdot \mathbf{A}^{IJ} \cdot \widetilde{\mathbf{G}}^J \cdot \widetilde{\mathbf{M}}^J. \tag{2.1.15}$$

The potential energy of the system equals the sum of the two interaction energies:

$$\widetilde{U}_{dd} = \widetilde{U}^{IJ} + \widetilde{U}^{JI}. \tag{2.1.16}$$

Given the orientation, magnetization, and shape of a pair of particles, the potential energy can be calculated at various relative positions of the particles to produce an energy landscape. In Figure 2.1, the dimensionless dipolar interaction energy ($\widetilde{U}_{dd}$) is plotted in particle I space. To plot in I space, a grid of positions around particle I on the particle I coordinate xy-plane is produced, excluding positions where the particles I and J would overlap. This grid is then transformed to lab space, the potential energy is calculated with particle J positioned at each point on the grid, and the grid is transformed back to particle I space for plotting.

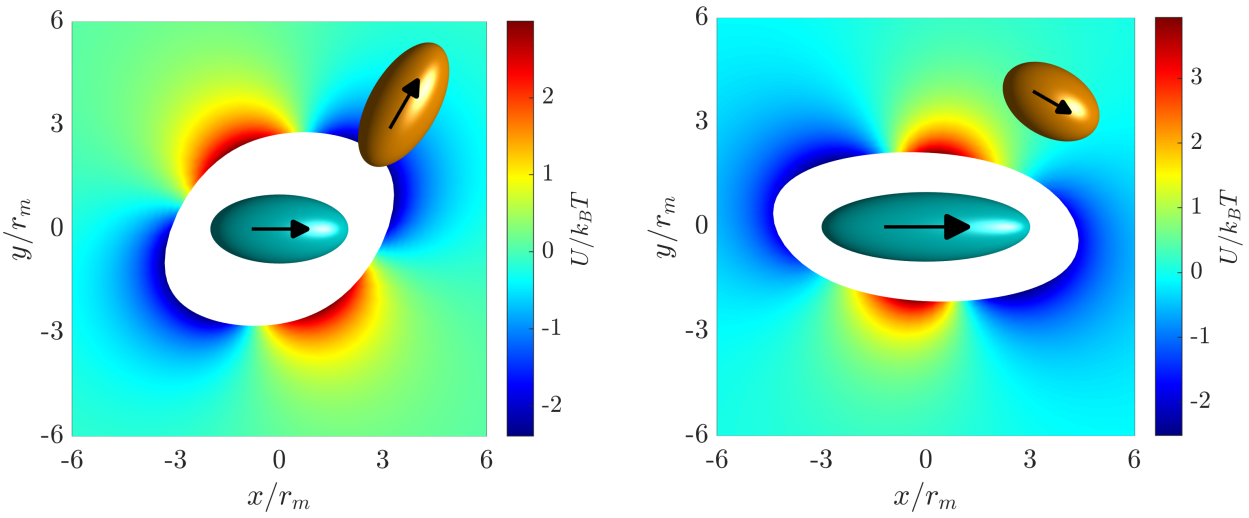

(a) Aspect ratios 2:1:1 and 2:1:1

(b) Aspect ratios 3:1:1 and 1.5:1:1

Figure 2.1: Dipolar interaction energy between particles I and J. For both pairs, magnetizations are $\widetilde{\mathbf{M}}^I = \widetilde{\mathbf{M}}^J = (1, 0, 0)$ and $\beta_s = 10$.

2.2 Analytically Calculated Force

The interaction energy between two magnetized ellipsoids results in a force pushing each particle towards a lower energy position. This force equals the negative gradient of energy with respect to particle position. For example, the force on particle J can be found by taking the negative gradient of the dipolar interaction energy with respect to the position of particle J. This theory is summarized for both particles by

$$\mathbf{F}_{dd}^J = -\nabla_J U_{dd}, \quad \mathbf{F}_{dd}^I = -\nabla_I U_{dd}, \tag{2.2.1}$$

where $\mathbf{F}_{dd}^J$ and $\mathbf{F}_{dd}^I$ are the dipolar interaction forces on particles J and I, respectively. The gradient operator with respect to each particle is defined as

$$\nabla_J = \left(\frac{\delta}{\delta x_J}, \frac{\delta}{\delta y_J}, \frac{\delta}{\delta z_J} \right), \quad \nabla_I = \left(\frac{\delta}{\delta x_I}, \frac{\delta}{\delta y_I}, \frac{\delta}{\delta z_I} \right). \tag{2.2.2}$$

Using equation (2.1.16) in equation (2.2.1) results in

$$\mathbf{F}_{dd}^J = -\nabla_J U^{IJ} - \nabla_J U^{JI}, \quad \mathbf{F}_{dd}^I = -\nabla_I U^{IJ} - \nabla_I U^{JI}. \tag{2.2.3}$$

The above equations imply the need for four gradient calculations to find the total force on both particles. However, the gradient operators with respect to the positions of the two particles can be related according to

$$\nabla_J = -\mathbf{A}^{JI} \nabla_I, \quad \nabla_I = -\mathbf{A}^{IJ} \nabla_J. \tag{2.2.4}$$

Applying this to equation (2.2.3) yields

$$\mathbf{F}_{dd}^{J} = -\nabla_J U^{IJ} + \mathbf{A}^{JI}\nabla_I U^{JI}, \quad \mathbf{F}_{dd}^{I} = \mathbf{A}^{IJ}\nabla_J U^{IJ} - \nabla_I U^{JI}. \tag{2.2.5}$$

To curtail computational costs, the evaluation of $\mathbf{F}_{dd}^{I}$ reduces to

$$\mathbf{F}_{dd}^{I} = -\mathbf{A}^{IJ}(-\nabla_J U^{IJ} + \mathbf{A}^{JI}\nabla_I U^{JI}) = -\mathbf{A}^{IJ}\mathbf{F}_{dd}^{J} \tag{2.2.6}$$

Thus, once the force on one particle is calculated, the force on the other particle can be found by negating and transforming the result.

The process for finding $\nabla_J U^{IJ}$ is shown below. The corresponding calculation for $\nabla_I U^{JI}$ follows a similar procedure. From equation (2.1.5),

$$\nabla_J U^{IJ} = \nabla_J \left(-\left(\frac{3m^J m^I}{8\pi\mu_0}\right) \widetilde{\mathbf{M}}^J \cdot \mathbf{A}^{JI} \cdot \mathbf{G}^I \cdot \widetilde{\mathbf{M}}^I \right). \tag{2.2.7}$$

Because only the Green tensor varies with position, this reduces to

$$\nabla_J U^{IJ} = -\left(\frac{3m^J m^I}{8\pi\mu_0}\right) \widetilde{\mathbf{M}}^J \cdot \mathbf{A}^{JI} \cdot \nabla_J \mathbf{G}^I \cdot \widetilde{\mathbf{M}}^I. \tag{2.2.8}$$

From Appendix B, gradient of the Green tensor equals

$$\frac{\delta}{\delta x_k} G_{ij} = \delta_{ij} F_{r_j}(\xi) \frac{\delta\xi}{\delta x_k} + \delta_{jk} F_{r_j}(\xi) \frac{\delta\xi}{\delta x_i} + x_j \frac{\delta F_{r_j}(\xi)}{\delta\xi} \frac{\delta\xi}{\delta x_k} \frac{\delta\xi}{\delta x_i} + x_j F_{r_j}(\xi) \frac{\delta^2\xi}{\delta x_i \delta x_k}, \tag{2.2.9}$$

where x_i is the position of particle J in direction i, and ξ is the ellipsoidal coordinate of particle J with respect to particle I.

The dimensionless analysis of the the energy gradient follows below. The dimensionless gradient operator is defined as

$$\widetilde{\nabla} = \left(\frac{\delta}{\delta\widetilde{x}}, \frac{\delta}{\delta\widetilde{y}}, \frac{\delta}{\delta\widetilde{z}} \right), \tag{2.2.10}$$

which relates to the extensive gradient operator as follows:

$$\nabla = \left(\frac{\delta}{\delta x}, \frac{\delta}{\delta y}, \frac{\delta}{\delta z} \right) = \left(\frac{\delta}{\delta\widetilde{x}}\frac{\delta\widetilde{x}}{\delta x}, \frac{\delta}{\delta\widetilde{y}}\frac{\delta\widetilde{y}}{\delta y}, \frac{\delta}{\delta\widetilde{z}}\frac{\delta\widetilde{z}}{\delta z} \right) = \left(\frac{\delta}{\delta\widetilde{x}}\frac{1}{r_m}, \frac{\delta}{\delta\widetilde{y}}\frac{1}{r_m}, \frac{\delta}{\delta\widetilde{z}}\frac{1}{r_m} \right) = \frac{1}{r_m}\widetilde{\nabla}. \tag{2.2.11}$$

Appendix C finds the dimensionless form of the Green tensor gradient as

$$\nabla\mathbf{G} = \frac{1}{r_m^4}\widetilde{\nabla}\widetilde{\mathbf{G}}. \tag{2.2.12}$$

Applying these relations to equation (2.2.8) yields

$$\frac{1}{r_m}\widetilde{\nabla}_J\widetilde{U}^{IJ} = -\left(\frac{3m^J m^I}{8\pi\mu_0 k_B T}\right)\widetilde{\mathbf{M}}^J\cdot\mathbf{A}^{JI}\cdot\frac{1}{r_m^4}\widetilde{\nabla}_J\widetilde{\mathbf{G}}^I\cdot\widetilde{\mathbf{M}}^I,$$

$$\widetilde{\nabla}_J\widetilde{U}^{IJ} = -\left(\frac{3m^J m^I}{8\pi\mu_0 r_m^3 k_B T}\right)\widetilde{\mathbf{M}}^J\cdot\mathbf{A}^{JI}\cdot\widetilde{\nabla}_{IJ}\widetilde{\mathbf{G}}^I\cdot\widetilde{\mathbf{M}}^I. \tag{2.2.13}$$

Applying the definition of the dipolar interaction parameter β from equation (2.1.12) gives

$$\widetilde{\nabla}_J\widetilde{U}^{IJ} = -\beta\cdot\widetilde{\mathbf{M}}^J\cdot\mathbf{A}^{JI}\cdot\widetilde{\nabla}_J\widetilde{\mathbf{G}}^I\cdot\widetilde{\mathbf{M}}^I. \tag{2.2.14}$$

For the total force on particle J, applying the above equation and the corresponding evaluation of $\nabla_I U^{JI}$ to equation (2.2.5) yields

$$\widetilde{\mathbf{F}}^J_{dd} = \beta\cdot\widetilde{\mathbf{M}}^J\cdot\mathbf{A}^{JI}\cdot\widetilde{\nabla}_J\widetilde{\mathbf{G}}^I\cdot\widetilde{\mathbf{M}}^I - \mathbf{A}^{JI}(\beta\cdot\widetilde{\mathbf{M}}^I\cdot\mathbf{A}^{IJ}\cdot\widetilde{\nabla}_I\widetilde{\mathbf{G}}^J\cdot\widetilde{\mathbf{M}}^J). \tag{2.2.15}$$

The total force on particle J can be plotted in particle I coordinates on a particle I space grid to produce a force field continuously perpendicular to the equipotential lines of the dipolar interaction energy. This perpendicular property of force results from its definition as the gradient of energy. In Figure 2.2, a dipolar interaction force field is plotted over the associated dipolar interaction energy.

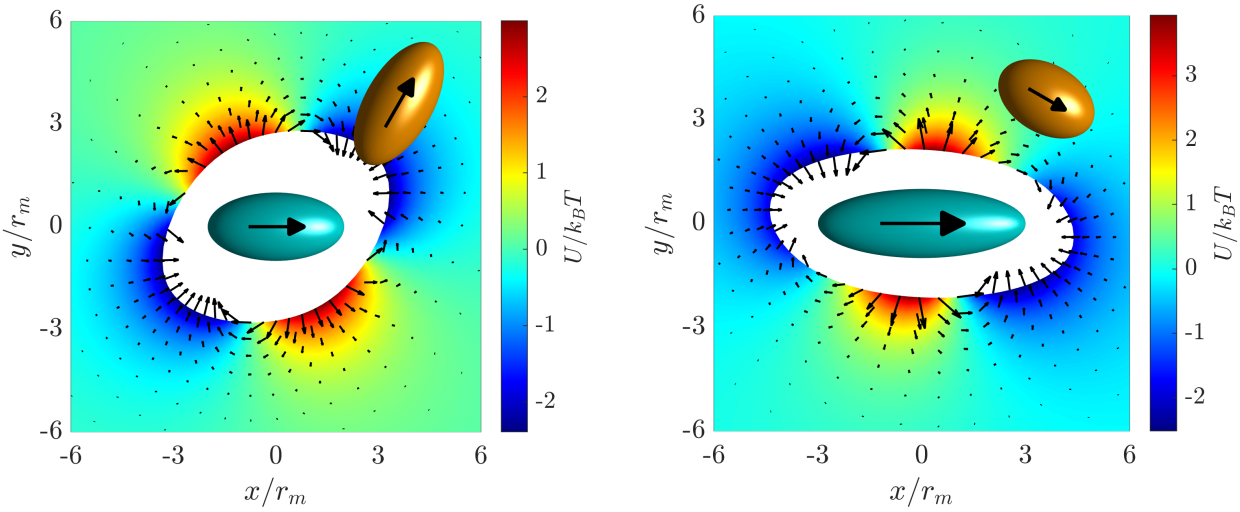

(a) Aspect ratios 2:1:1 and 2:1:1

(b) Aspect ratios 3:1:1 and 1.5:1:1

Figure 2.2: Dipolar interaction force between particles I and J. For both pairs, magnetizations are $\widetilde{\mathbf{M}}^I = \widetilde{\mathbf{M}}^J = (1,0,0)$ and $\beta_s = 10$.

2.3 Numerically Calculated Force

Using the definition of gradient, the dipolar interaction force can be calculated numerically to corroborate the analytical calculations. For example, the force on particle J equals the negative gradient of the energy with respect to particle J position:

$$\widetilde{\mathbf{F}}_{dd}^{J} = -\widetilde{\nabla}_{J}\widetilde{U}_{dd} = \left(-\frac{\delta\widetilde{U}_{dd}}{\delta\widetilde{x}_{J}}, -\frac{\delta\widetilde{U}_{dd}}{\delta\widetilde{y}_{J}}, -\frac{\delta\widetilde{U}_{dd}}{\delta\widetilde{z}_{J}} \right). \tag{2.3.1}$$

The partial derivative of the dipolar interaction energy along any axis can be estimated by determining the energy at the particle J position plus a displacement d along the axis and minus a displacement d along the axis, then by calculating the slope between these two points:

$$\begin{aligned}
\frac{\delta\widetilde{U}_{dd}}{\delta\widetilde{x}_{J}} &\approx \frac{\widetilde{U}_{dd}\left(\widetilde{x}^{J}+d,\widetilde{y}^{J},\widetilde{z}^{I}\right)-\widetilde{U}_{dd}\left(\widetilde{x}^{J}-d,\widetilde{y}^{J},\widetilde{z}^{J}\right)}{2d}, \\
\frac{\delta\widetilde{U}_{dd}}{\delta\widetilde{y}_{J}} &\approx \frac{\widetilde{U}_{dd}\left(\widetilde{x}^{J},\widetilde{y}^{J}+d,\widetilde{z}^{I}\right)-\widetilde{U}_{dd}\left(\widetilde{x}^{J},\widetilde{y}^{J}-d,\widetilde{z}^{J}\right)}{2d}, \\
\frac{\delta\widetilde{U}_{dd}}{\delta\widetilde{z}_{J}} &\approx \frac{\widetilde{U}_{dd}\left(\widetilde{x}^{J},\widetilde{y}^{J},\widetilde{z}^{I}+d\right)-\widetilde{U}_{dd}\left(\widetilde{x}^{J},\widetilde{y}^{J},\widetilde{z}^{J}-d\right)}{2d}.
\end{aligned} \tag{2.3.2}$$

The step size d must be small enough to accurately estimate the partial derivative, but large enough to avoid significant computational round-off errors. The dipolar interaction force on particle I can be calculated by varying the position of particle I instead of particle J.

Recall that because force has direction, these calculations necessarily produce a vector defined in a certain coordinate system. In the case of numerical force calculations, this depends on the choice of axes on which to vary particle position. In this work, particle J position is varied along the lab coordinate axes, then the results are transformed to particle I space for plotting.

As shown in Figure 2.3, numerical force fields can be plotted in the same manner as analytical force fields. Figure 2.4 demonstrates that the two methods produce the same vector fields.

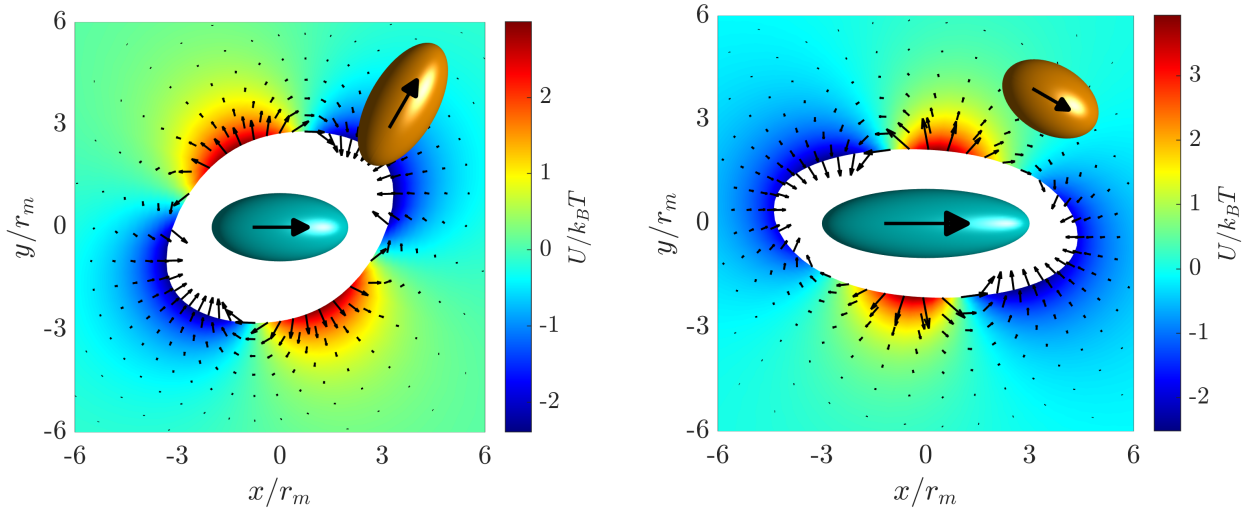

(a) Aspect ratios 2:1:1 and 2:1:1

(b) Aspect ratios 3:1:1 and 1.5:1:1

Figure 2.3: Numerically calculated ($d = 10^{-6} \cdot r_m$) dipolar interaction force between particles I and J. For both pairs, magnetizations are $\widetilde{\mathbf{M}}^I = \widetilde{\mathbf{M}}^J = (1, 0, 0)$ and $\beta_s = 10$.

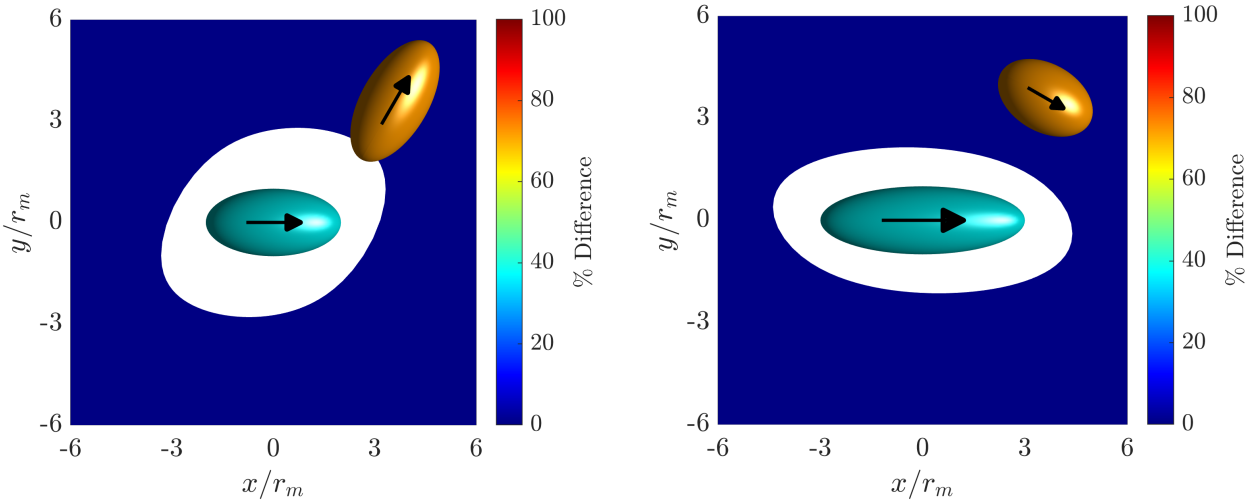

(a) Aspect ratios 2:1:1 and 2:1:1

(b) Aspect ratios 3:1:1 and 1.5:1:1

Figure 2.4: Direct comparison of analytical and numerical force calculation methods.

2.4 Analytically Calculated Torque

The interaction energy between a magnetic dipole and a magnetic field results in a torque that rotates the dipole towards a lower energy orientation. The lowest energy orientation occurs when the dipole aligns with the local field. For example, the force on particle J equals the negative gradient of the dipolar interaction energy with respect to the orientation of particle J. This concept is summarized for both particles by

$$\tau_{dd}^{J} = -\frac{\delta U_{dd}}{\delta \mathbf{\Phi}^{JI}}, \quad \tau_{dd}^{I} = -\frac{\delta U_{dd}}{\delta \mathbf{\Phi}^{IJ}}, \tag{2.4.1}$$

where τ_{dd}^{J} and τ_{dd}^{I} are the dipolar interaction torques on particle J and particle I, respectively, $\mathbf{\Phi}^{JI}$ is the orientation of particle J relative to particle I, and $\mathbf{\Phi}^{IJ}$ is the orientation of particle I relative to particle J. Using equation (2.1.16) in equation (2.4.1) results in

$$\tau_{dd}^{J} = -\frac{\delta U^{IJ}}{\delta \mathbf{\Phi}^{JI}} - \frac{\delta U^{JI}}{\delta \mathbf{\Phi}^{JI}}, \quad \tau_{dd}^{I} = -\frac{\delta U^{IJ}}{\delta \mathbf{\Phi}^{IJ}} - \frac{\delta U^{JI}}{\delta \mathbf{\Phi}^{IJ}}, \tag{2.4.2}$$

As with force, the partial derivatives with with respect to the orientations of the two particles can be related according to

$$\frac{\delta}{\delta \mathbf{\Phi}^{JI}} = -\mathbf{A}^{JI}\frac{\delta}{\delta \mathbf{\Phi}^{IJ}}, \quad \frac{\delta}{\delta \mathbf{\Phi}^{IJ}} = -\mathbf{A}^{IJ}\frac{\delta}{\delta \mathbf{\Phi}^{JI}}. \tag{2.4.3}$$

Applying this to equation (2.4.2) yields

$$\tau_{dd}^{J} = -\frac{\delta U^{IJ}}{\delta \mathbf{\Phi}^{JI}} + \mathbf{A}^{JI}\frac{\delta U^{JI}}{\delta \mathbf{\Phi}^{IJ}}, \quad \tau_{dd}^{I} = \mathbf{A}^{IJ}\frac{\delta U^{IJ}}{\delta \mathbf{\Phi}^{JI}} - \frac{\delta U^{JI}}{\delta \mathbf{\Phi}^{IJ}}. \tag{2.4.4}$$

To curtail computational costs, the evaluation of τ_{dd}^{I} reduces to

$$\tau_{dd}^{I} = -\mathbf{A}^{IJ}\left(-\frac{\delta U^{IJ}}{\delta \mathbf{\Phi}^{JI}} + \mathbf{A}^{JI}\frac{\delta U^{JI}}{\delta \mathbf{\Phi}^{IJ}}\right) = -\mathbf{A}^{IJ}\tau_{dd}^{J}. \tag{2.4.5}$$

Again, as with force, once the torque on one particle is calculated, the torque on the other particle can be found by negating and transforming the result.

The process for finding $\delta U^{IJ}/\delta \mathbf{\Phi}^{JI}$ is shown below. The corresponding calculation for $\delta U^{JI}/\delta \mathbf{\Phi}^{IJ}$ follows a similar procedure. Because this work uses quaternions to represent orientation, these equations are transformed to quaternion derivatives as follows:

$$\frac{\delta U^{IJ}}{\delta \mathbf{\Phi}^{JI}} = \mathbf{\Psi}^{JI,T}\frac{\delta U^{IJ}}{\delta \mathbf{q}^{JI}} \tag{2.4.6}$$

where $\mathbf{q}^{JI} = \left(q_0^{JI}, q_1^{JI}, q_2^{JI}, q_3^{JI}\right)$ is the quaternion of particle J relative to particle I, and $\mathbf{\Psi}^{JI,T}$ is the transpose of $\mathbf{\Psi}^{JI}$. In a more explicit form, this equals

$$\frac{\delta U^{IJ}}{\delta \mathbf{\Phi}^{JI}} = \mathbf{\Psi}^{JI,T} \begin{bmatrix} \delta U^{IJ}/\delta q_0^{JI} \\ \delta U^{IJ}/\delta q_1^{JI} \\ \delta U^{IJ}/\delta q_2^{JI} \\ \delta U^{IJ}/\delta q_3^{JI} \end{bmatrix}. \tag{2.4.7}$$

As defined by Delong [14], $\mathbf{\Psi}^{JI} \equiv \delta\mathbf{q}/\delta\mathbf{\Phi}$ has several useful when properties attempting to relate rotational motion and quaternions. For the general quaternion $\mathbf{q} = (q_0, q_1, q_2, q_3)$, $\mathbf{\Psi}$ and $\mathbf{\Psi}^T$ respectively follow

$$\mathbf{\Psi} = \frac{1}{2} \begin{bmatrix} q_1 & q_2 & q_3 \\ -q_0 & -q_3 & q_2 \\ q_3 & -q_0 & -q_1 \\ -q_2 & q_1 & -q_0 \end{bmatrix}, \tag{2.4.8}$$

$$\mathbf{\Psi}^T = \frac{1}{2} \begin{bmatrix} q_1 & -q_0 & q_3 & -q_2 \\ q_2 & -q_3 & -q_0 & q_1 \\ q_3 & q_2 & -q_1 & -q_0 \end{bmatrix}. \tag{2.4.9}$$

Appendix D shows the derivation of these identities. Note that Evans [12] finds a similar matrix for $\mathbf{\Psi}$ with the same placement of the quaternion parameters but different signs. This results from equation (1.2.2) in this report, which defines quaternions slightly differently Evans. If one uses the quaternions as defined by Evans in the derivation shown in Appendix D, one will find $\mathbf{\Psi}$ as given by Evans.

Substituting equation (2.1.5) for U^{IJ} in equation (2.4.6) yields

$$\frac{\delta U^{IJ}}{\delta \mathbf{\Phi}^{JI}} = \mathbf{\Psi}^{JI} \frac{\delta}{\delta \mathbf{q}^{JI}} \left(- \left(\frac{3m^J m^I}{8\pi\mu_0} \right) \cdot \widetilde{\mathbf{M}}^J \cdot \mathbf{A}^{JI} \cdot \mathbf{G}^I \cdot \widetilde{\mathbf{M}}^I \right). \tag{2.4.10}$$

Because only the transformation matrix varies with orientation, this simplifies to

$$\frac{\delta U^{IJ}}{\delta \mathbf{\Phi}^{JI}} = -\mathbf{\Psi}^{JI} \left(\frac{3m^J m^I}{8\pi\mu_0} \right) \cdot \widetilde{\mathbf{M}}^J \cdot \frac{\delta \mathbf{A}^{JI}}{\delta \mathbf{q}^{JI}} \cdot \mathbf{G}^I \cdot \widetilde{\mathbf{M}}^I. \tag{2.4.11}$$

Since polynomial functions of the quaternion parameters define the transformation matrices, their partial derivatives with respect to quaternions are trivial to calculate, as shown below. The partial derivative of a transformation matrix $\mathbf{A}$ defined by equation (1.2.8) with respect to the each of the quaternion parameters equals

$$\begin{aligned} \frac{\delta \mathbf{A}}{\delta q_0} &= \begin{bmatrix} 2q_0 & -2q_3 & 2q_2 \\ 2q_3 & 2q_0 & -2q_1 \\ -2q_2 & 2q_1 & 2q_0 \end{bmatrix}, \frac{\delta \mathbf{A}}{\delta q_1} = \begin{bmatrix} 2q_1 & 2q_2 & 2q_3 \\ 2q_2 & -2q_1 & -2q_0 \\ 2q_3 & 2q_0 & -2q_1 \end{bmatrix}, \\ \frac{\delta \mathbf{A}}{\delta q_2} &= \begin{bmatrix} -2q_2 & 2q_1 & 2q_0 \\ 2q_1 & 2q_2 & 2q_3 \\ -2q_0 & 2q_3 & -2q_2 \end{bmatrix}, \frac{\delta \mathbf{A}}{\delta q_3} = \begin{bmatrix} -2q_3 & -2q_0 & 2q_1 \\ 2q_0 & -2q_3 & 2q_2 \\ 2q_1 & 2q_2 & 2q_3 \end{bmatrix}. \end{aligned} \tag{2.4.12}$$

Because quaternions have no units, dimensionless analysis of torque follows the same procedure and produces the same outcome as energy.

$$\frac{\delta\widetilde{U}^{IJ}}{\delta\mathbf{\Phi}^{JI}} = -\mathbf{\Psi}^{JI}\left(\frac{3m^Jm^I}{8\pi\mu_0 r_m^3 k_B T}\right)\cdot\widetilde{\mathbf{M}}^J\cdot\frac{\delta\mathbf{A}^{JI}}{\delta\mathbf{q}^{JI}}\cdot\widetilde{\mathbf{G}}^I\cdot\widetilde{\mathbf{M}}^I,$$

$$\frac{\delta\widetilde{U}^{IJ}}{\delta\mathbf{\Phi}^{JI}} = -\beta\cdot\mathbf{\Psi}^{JI}\cdot\widetilde{\mathbf{M}}^J\cdot\frac{\delta\mathbf{A}^{JI}}{\delta\mathbf{q}^{JI}}\cdot\widetilde{\mathbf{G}}^I\cdot\widetilde{\mathbf{M}}^I. \tag{2.4.13}$$

For the total torque on particle J, the above equation and the corresponding calculation for $\delta\widetilde{U}^{JI}/\delta\mathbf{\Phi}^{IJ}$ are substituted into equation (2.4.4), yielding

$$\widetilde{\tau}_{dd}^J = \beta\cdot\mathbf{\Psi}^{JI}\cdot\widetilde{\mathbf{M}}^J\cdot\frac{\delta\mathbf{A}^{JI}}{\delta\mathbf{q}^{JI}}\cdot\widetilde{\mathbf{G}}^I\cdot\widetilde{\mathbf{M}}^I - \mathbf{A}^{JI}(\beta\cdot\mathbf{\Psi}^{IJ}\cdot\widetilde{\mathbf{M}}^I\cdot\frac{\delta\mathbf{A}^{IJ}}{\delta\mathbf{q}^{IJ}}\cdot\widetilde{\mathbf{G}}^J\cdot\widetilde{\mathbf{M}}^J). \tag{2.4.14}$$

The dipolar interaction torque between two particles can also be calculated using the definition of torque resulting from a magnetic moment interacting with a magnetic field:

$$\tau = \mathbf{m}\times\mathbf{H}. \tag{2.4.15}$$

For example, the total dipolar interaction torque on particle J equals the sum of the torques from particle J's moment interacting with particle I's field and from particle I's moment interacting with particle J's field:

$$\tau_{dd}^J = \mathbf{m}^J\times\mathbf{H}^I - \mathbf{A}^{JI}(\mathbf{m}^I\times\mathbf{H}^J). \tag{2.4.16}$$

Note that because the latter term produces the torque on particle I in particle I space, the result must be negated and transformed to particle J space to find the effect on particle J. Using the definition of magnetic moment and equation (2.1.3) for H field,

$$\tau_{dd}^J = \left(\frac{3m^Jm^I}{8\pi\mu_0}\right)\widetilde{\mathbf{M}}^J\times\mathbf{A}^{JI}\cdot\mathbf{G}^I\cdot\widetilde{\mathbf{M}}^I - \mathbf{A}^{JI}\left(\left(\frac{3m^Jm^I}{8\pi\mu_0}\right)\widetilde{\mathbf{M}}^I\times\mathbf{A}^{IJ}\cdot\mathbf{G}^J\cdot\widetilde{\mathbf{M}}^J\right). \tag{2.4.17}$$

In dimensionless form,

$$\widetilde{\tau}_{dd}^J = \beta\cdot\widetilde{\mathbf{M}}^J\times\mathbf{A}^{JI}\cdot\widetilde{\mathbf{G}}^I\cdot\widetilde{\mathbf{M}}^I - \mathbf{A}^{JI}\left(\beta\cdot\widetilde{\mathbf{M}}^I\times\mathbf{A}^{IJ}\cdot\widetilde{\mathbf{G}}^J\cdot\widetilde{\mathbf{M}}^J\right). \tag{2.4.18}$$

This equation produces the same result as equation (2.4.14), which uses the quaternion derivative. In Figure 2.5, dipolar interaction torque fields are plotted where circles represent vectors pointing out of the page, and crosses represent vectors pointing into the page. The landscape beneath the symbols is the magnitude of the torque vector. The results from the cross product method (not shown) exactly match the results from the quaternion gradient method (shown).

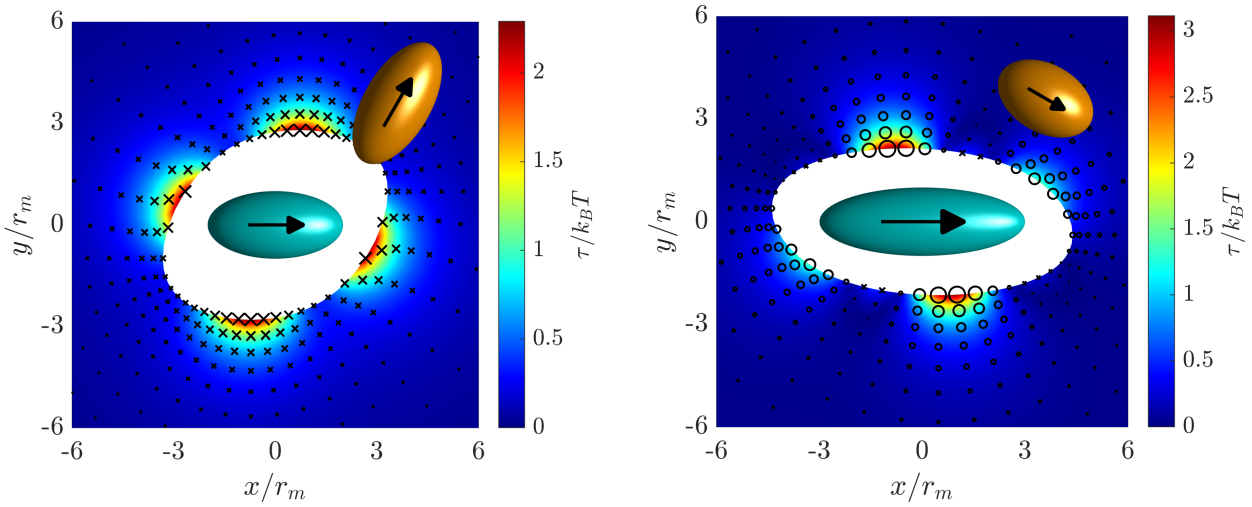

(a) Aspect ratios 2:1:1 and 2:1:1

(b) Aspect ratios 3:1:1 and 1.5:1:1

Figure 2.5: Dipolar interaction torque between particles I and J. For both pairs, magnetizations are $\widetilde{\mathbf{M}}^I = \widetilde{\mathbf{M}}^J = (1, 0, 0)$ and $\beta_s = 10$.

2.5 Numerically Calculated Torque

Numerical calculation of dipolar interaction torque follows a similar path as the numerical force calculation. Consider the dipolar interaction torque on particle J, which equals the negative quaternion gradient of energy with respect to particle J orientation:

$$\widetilde{\tau}_{dd}^J = -\mathbf{\Psi}^J \frac{\delta \widetilde{U}_{dd}}{\delta \mathbf{q}^J} = \mathbf{\Psi}^J \left(-\frac{\delta \widetilde{U}_{dd}}{\delta q_0^J}, -\frac{\delta \widetilde{U}_{dd}}{\delta q_1^J}, -\frac{\delta \widetilde{U}_{dd}}{\delta q_2^J}, -\frac{\delta \widetilde{U}_{dd}}{\delta q_3^J} \right). \tag{2.5.1}$$

The partial derivative of the dipolar interaction energy with respect to any quaternion can be estimated by determining the energy at the particle J position plus a displacement d of that quaternion and minus a displacement d of that quaternion, then by calculating the slope between these two points:

$$\begin{aligned}
\frac{\delta \widetilde{U}_{dd}}{\delta q_0^J} &\approx \frac{\widetilde{U}_{dd}\left(q_0^J + d, q_1^J, q_2^J, q_3^J\right) - \widetilde{U}_{dd}\left(q_0^J - d, q_1^J, q_2^J, q_3^J\right)}{2d}, \\
\frac{\delta \widetilde{U}_{dd}}{\delta q_1^J} &\approx \frac{\widetilde{U}_{dd}\left(q_0^J, q_1^J + d, q_2^J, q_3^J\right) - \widetilde{U}_{dd}\left(q_0^J, q_1^J - d, q_2^J, q_3^J\right)}{2d}, \\
\frac{\delta \widetilde{U}_{dd}}{\delta q_2^J} &\approx \frac{\widetilde{U}_{dd}\left(q_0^J, q_1^J, q_2^J + d, q_3^J\right) - \widetilde{U}_{dd}\left(q_0^J, q_1^J, q_2^J - d, q_3^J\right)}{2d}, \\
\frac{\delta \widetilde{U}_{dd}}{\delta q_3^J} &\approx \frac{\widetilde{U}_{dd}\left(q_0^J, q_1^J, q_2^J, q_3^J + d\right) - \widetilde{U}_{dd}\left(q_0^J, q_1^J, q_2^J, q_3^J - d\right)}{2d}.
\end{aligned} \tag{2.5.2}$$

Because torque has direction, these equations produce a vector in a certain coordinate space. For numerical torque calculations, this depends on the quaternion that is varied and associated $\mathbf{\Psi}$ matrix that is applied. The above equations produce a torque defined in particle J space. Numerical calculation of torque on particle I follows the same procedure as above and produces a result in particle I space. Figures 2.6 and 2.7 summarize the results.

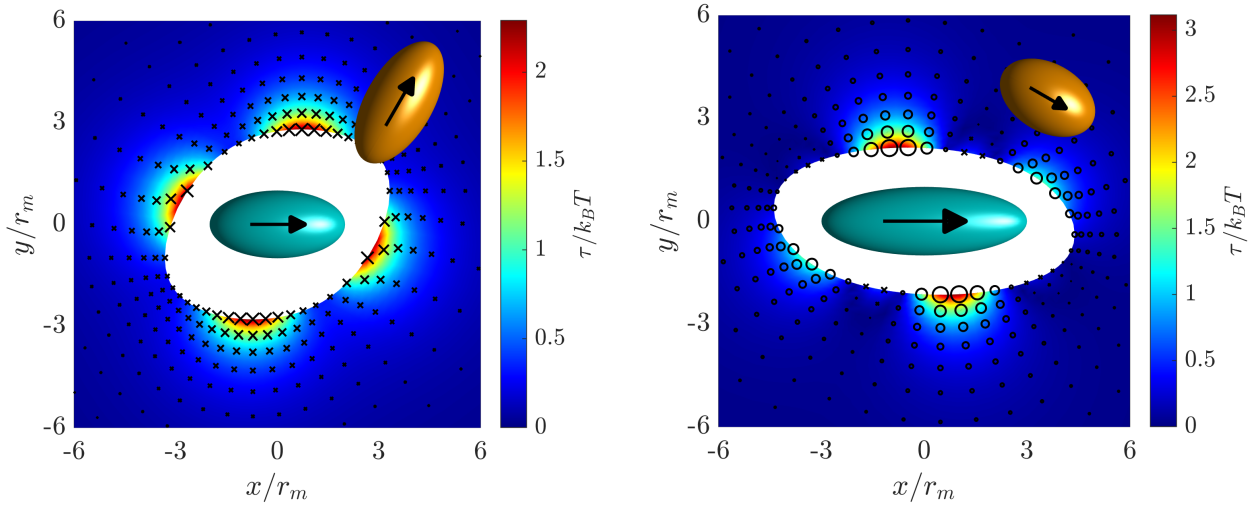

(a) Aspect ratios 2:1:1 and 2:1:1

(b) Aspect ratios 3:1:1 and 1.5:1:1

Figure 2.6: Numerically calculated ($d = 10^{-6} \cdot r_m$) dipolar interaction torque between particles I and J. For both pairs, magnetizations are $\widetilde{\mathbf{M}}^I = \widetilde{\mathbf{M}}^J = (1, 0, 0)$ and $\beta_s = 10$.

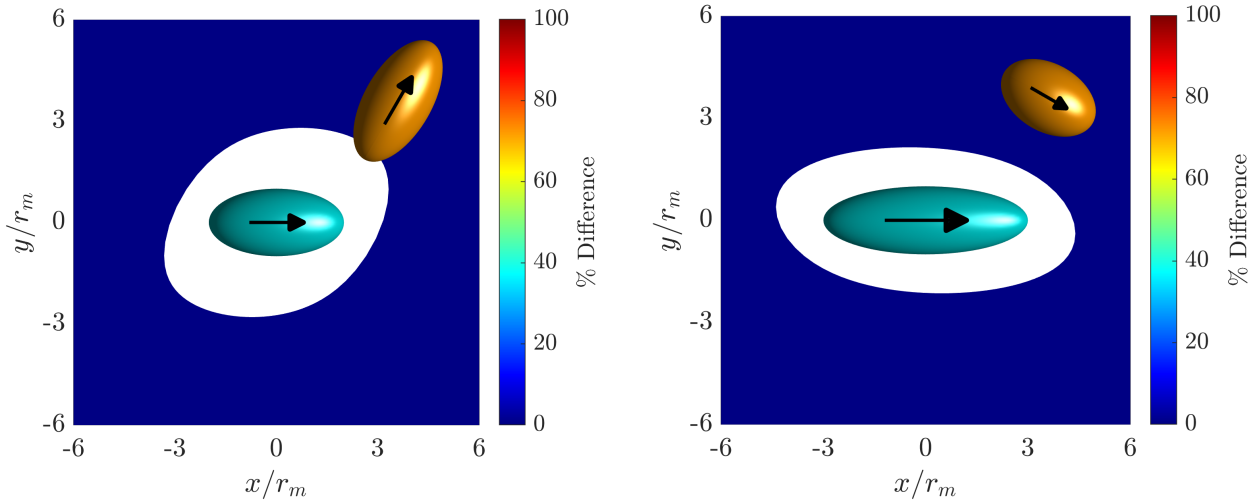

(a) Aspect ratios 2:1:1 and 2:1:1

(b) Aspect ratios 3:1:1 and 1.5:1:1

Figure 2.7: Direct comparison of analytical and numerical torque calculation methods.

2.6 Comparison with Point-Dipole Model

Dipolar interactions of spherical particles have been extensively studied and modeled using the point-dipole model. Because of the simplicity of spherical particles, these interactions pose much less of a challenge to analyze. Thus, the formulas describing these interactions offer themselves as simple method for corroborating the formulas derived in the past several sections of this report. To accomplish this, the formulas for ellipsoidal particles were applied to spherical particles, and the results were compared to those of the point-particle model.

First, according to Edwards [15], the dipolar interaction energy between spheres (modified to use the notation of this report) follows

$$U^{IJ} = \frac{\mu_0}{4\pi}\left(\frac{\mathbf{m}^I \cdot \mathbf{m}^J}{(x^{IJ})^3} - 3\frac{(\mathbf{m}^I \cdot \mathbf{x}^{IJ})(\mathbf{m}^J \cdot \mathbf{x}^{IJ})}{(x^{IJ})^5}\right) \tag{2.6.1}$$

where U^{IJ} is the interaction energy of particle J's dipole with particle I's field, $\mathbf{m}^I$ and $\mathbf{m}^J$ are the magnetic moments of particle I and particle J, respectively, $\mathbf{x}^{IJ}$ is the position of particle J relative to particle I in particle I space, and x^{IJ} is the magnitude of $\mathbf{x}^{IJ}$. Edwards defines the relationship between magnetic moment and magnetization as $\mathbf{m} = v_p\mathbf{M}$. Putting equation (2.6.1) in terms of magnetization and factoring out x^{IJ} yields

$$U^{IJ} = \frac{\mu_0 v_p^I v_p^J}{4\pi(x^{IJ})^3}\left(\mathbf{M}^I \cdot \mathbf{M}^J - 3(\mathbf{M}^I \cdot \hat{\mathbf{x}}^{IJ})(\mathbf{M}^J \cdot \hat{\mathbf{x}}^{IJ})\right), \tag{2.6.2}$$

where $\hat{\mathbf{x}}^{IJ}$ is the unit vector in the direction of $\mathbf{x}^{IJ}$. Factoring out the magnitude M of the magnetization vector and using the identity $m = \mu_0 v_p M$ gives

$$U^{IJ} = \frac{m^J m^I}{4\pi\mu_0(x^{IJ})^3}\left(\widetilde{\mathbf{M}}^I \cdot \widetilde{\mathbf{M}}^J - 3(\widetilde{\mathbf{M}}^I \cdot \hat{\mathbf{x}}^{IJ})(\widetilde{\mathbf{M}}^J \cdot \hat{\mathbf{x}}^{IJ})\right). \tag{2.6.3}$$

In dimensionless form, the dipolar interaction energy follows

$$\widetilde{U}^{IJ} = \frac{m^J m^I}{4\pi\mu_0 r_m^3 k_B T}\frac{1}{(\widetilde{x}^{IJ})^3}\left(\widetilde{\mathbf{M}}^I \cdot \widetilde{\mathbf{M}}^J - 3(\widetilde{\mathbf{M}}^I \cdot \hat{\mathbf{x}}^{IJ})(\widetilde{\mathbf{M}}^J \cdot \hat{\mathbf{x}}^{IJ})\right). \tag{2.6.4}$$

As originally given by equation equation (2.1.12),

$$\beta \equiv \frac{3m^J m^I}{8\pi\mu_0 r_m^3 k_B T} \tag{2.1.12}$$

defines the dipolar interaction parameter. Substituting this into equation (2.6.1) yields

$$\widetilde{U}^{IJ} = \frac{2}{3}\beta\frac{1}{(\widetilde{x}^{IJ})^3}\left(\widetilde{\mathbf{M}}^I \cdot \widetilde{\mathbf{M}}^J - 3(\widetilde{\mathbf{M}}^I \cdot \hat{\mathbf{x}}^{IJ})(\widetilde{\mathbf{M}}^J \cdot \hat{\mathbf{x}}^{IJ})\right). \tag{2.6.5}$$

For spheres, the results from this equation should match those from equation (2.1.11).

Next, according to Zhao [16], the dipolar interaction force between spheres (modified to use the notation of this report) follows

$$\mathbf{F}^{IJ} = \frac{3\mu_0}{4\pi}\left(\frac{(\mathbf{m}^I\cdot\mathbf{x}^{IJ})\mathbf{m}^J + (\mathbf{m}^J\cdot\mathbf{x}^{IJ})\mathbf{m}^I + (\mathbf{m}^I\cdot\mathbf{m}^J)\mathbf{x}^{IJ}}{(x^{IJ})^5} - 5\frac{(\mathbf{m}^I\cdot\mathbf{x}^{IJ})(\mathbf{m}^J\cdot\mathbf{x}^{IJ})}{(x^{IJ})^7}\mathbf{x}^{IJ}\right) \tag{2.6.6}$$

where $\mathbf{F}^{IJ}$ is the dipolar interaction force on particle J. Factoring out magnetic moment and magnitude M from magnetization, applying the definition of magnetic moment, factoring out x^{IJ}, and making force dimensionless yields

$$\widetilde{\mathbf{F}}^{IJ} = \frac{3m^Jm^I}{4\pi\mu_0 r_m^3 k_B T}\frac{1}{(\widetilde{x}^{IJ})^4}\left((\widetilde{\mathbf{M}}^I\cdot\hat{\mathbf{x}}^{IJ})\widetilde{\mathbf{M}}^J + (\widetilde{\mathbf{M}}^J\cdot\hat{\mathbf{x}}^{IJ})\widetilde{\mathbf{M}}^I + (\widetilde{\mathbf{M}}^I\cdot\widetilde{\mathbf{M}}^J)\hat{\mathbf{x}}^{IJ} - 5(\widetilde{\mathbf{M}}^I\cdot\hat{\mathbf{x}}^{IJ})(\widetilde{\mathbf{M}}^J\cdot\hat{\mathbf{x}}^{IJ})\hat{\mathbf{x}}^{IJ}\right). \tag{2.6.7}$$

Substituting in the parameter β gives

$$\widetilde{\mathbf{F}}^{IJ} = 2\beta\frac{1}{(\widetilde{x}^{IJ})^4}\left((\widetilde{\mathbf{M}}^I\cdot\hat{\mathbf{x}}^{IJ})\widetilde{\mathbf{M}}^J + (\widetilde{\mathbf{M}}^J\cdot\hat{\mathbf{x}}^{IJ})\widetilde{\mathbf{M}}^I + (\widetilde{\mathbf{M}}^I\cdot\widetilde{\mathbf{M}}^J)\hat{\mathbf{x}}^{IJ} - 5(\widetilde{\mathbf{M}}^I\cdot\hat{\mathbf{x}}^{IJ})(\widetilde{\mathbf{M}}^J\cdot\hat{\mathbf{x}}^{IJ})\hat{\mathbf{x}}^{IJ}\right). \tag{2.6.8}$$

For spheres, the results from this equation should match those from equation (2.2.15).

Next, according to Zhao [16], the dipolar interaction torque between spheres (modified to use the notation of this report) follows

$$\tau^{IJ} = \frac{\mu_0}{4\pi}\left(\frac{\mathbf{m}^I\times\mathbf{m}^J}{(x^{IJ})^3} + 3\frac{(\mathbf{m}^I\cdot\mathbf{x}^{IJ})(\mathbf{m}^J\times\mathbf{x}^{IJ})}{(x^{IJ})^5}\right) \tag{2.6.9}$$

where τ^{IJ} is the dipolar interaction torque on particle J. Factoring out magnetic moment and magnitude M from magnetization, applying the definition of magnetic moment, factoring out x^{IJ}, and making torque dimensionless yields

$$\widetilde{\tau}^{IJ} = \frac{m^Jm^I}{4\pi\mu_0 r_m^3 k_B T}\frac{1}{(\widetilde{x}^{IJ})^3}\left(\widetilde{\mathbf{M}}^I\times\widetilde{\mathbf{M}}^J + 3(\widetilde{\mathbf{M}}^I\cdot\hat{\mathbf{x}}^{IJ})(\widetilde{\mathbf{M}}^J\times\hat{\mathbf{x}}^{IJ})\right). \tag{2.6.10}$$

Substituting in the parameter β gives

$$\widetilde{\tau}^{IJ} = \frac{2}{3}\beta\frac{1}{(\widetilde{x}^{IJ})^3}\left(\widetilde{\mathbf{M}}^I\times\widetilde{\mathbf{M}}^J + 3(\widetilde{\mathbf{M}}^I\cdot\hat{\mathbf{x}}^{IJ})(\widetilde{\mathbf{M}}^J\times\hat{\mathbf{x}}^{IJ})\right). \tag{2.6.11}$$

For spheres, the results from this equation should match those from equations (2.4.13).

Figure 2.8 compares the results from the ellipsoid-dipole model and point-dipole model using spherical particles. They match well.

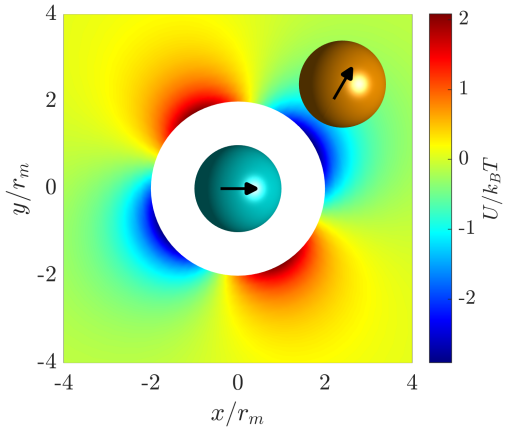

(a) Energy using ellipsoid-dipole model

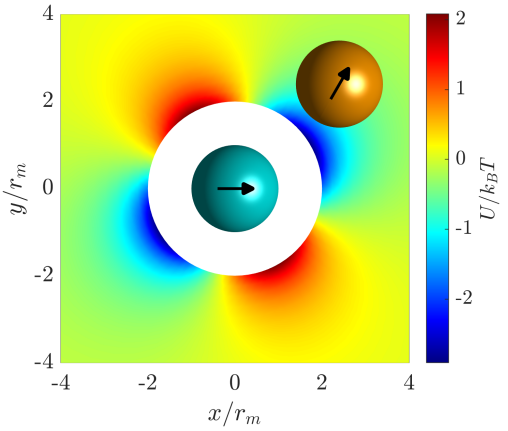

(b) Energy using point-dipole model

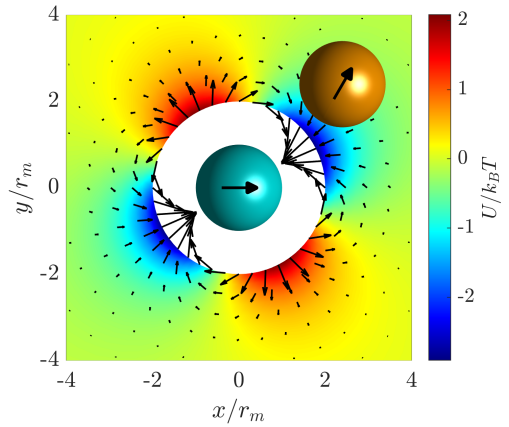

(c) Force using ellipsoid-dipole model

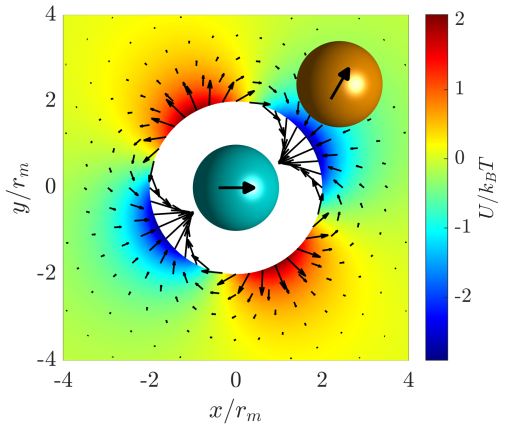

(d) Force using point-dipole model

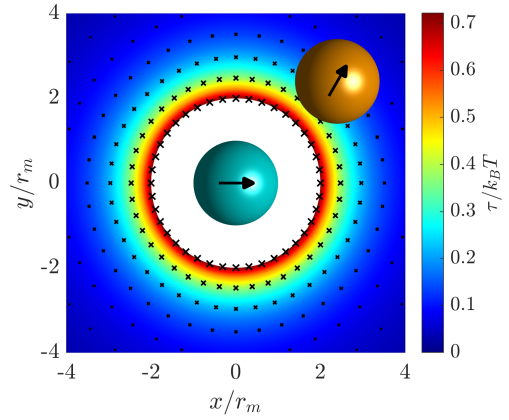

(e) Torque using ellipsoid-dipole model

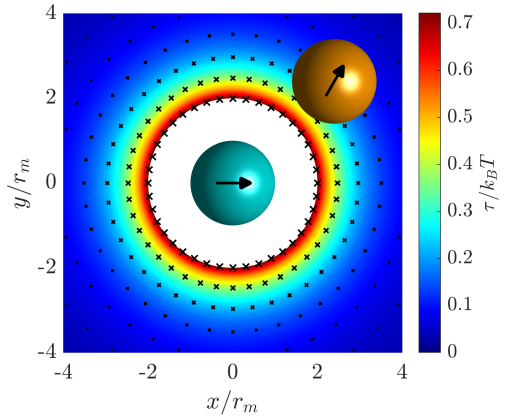

(f) Torque using point-dipole model

Figure 2.8: Comparison of ellipsoid-dipole model and point-dipole model dynamics. Magnetizations are $\widetilde{\mathbf{M}}^I = \widetilde{\mathbf{M}}^J = (1, 0, 0)$ and $\beta_s = 10$.

Chapter 3

Brownian Dynamics

3.1 Electrostatic Repulsion

When suspended in a liquid with a high dielectric constant (such as water), colloidal particles experience negative surface charging. At close range, this causes mutual electrostatic repulsion of the particles. The magnitude of charging depends on the properties of both the colloid and the solvent. Furthermore, if the solution contains dissolved ions, the charged molecules congregate around the particle surfaces, enhancing the repulsion. The Derjaguin approximation models electrostatic repulsion between colloids when the diameter of the particles significantly surpasses the range of the interactions. According to this approximation as described by Israelachvili [17], the electrostatic energy U_e between two spheres follows

$$U_e = \frac{r^I r^J}{r^I + r^J} \zeta e^{-\kappa D}, \tag{3.1.1}$$

where r^I and r^J are the radii of particles I and J, respectively, D is the minimum separation distance between the surfaces of the particles, $\zeta = 64\pi\epsilon_0\epsilon(k_BT/e)^2 tanh^2(ze\psi_0/4k_BT)$ is a parameter that determines the strength of the interaction according to particle surface properties, and $\kappa = (\Sigma\rho_{\inf i} e^2 z_i^2/\epsilon_0\epsilon k_B T)^{-1/2}$ is the inverse of the Debye length κ^{-1}, a parameter that determines the extensiveness of the interaction depending on solution properties.

Because ellipsoids do not have constant radii, the fractional term in Equation (3.1.1) must be replaced by more complex term that accounts for the curvature of the particles near the point of minimum separation. This term depends on the Guassian curvature K and mean curvature H of both particles, and surface coordinate system mismatch angle ϕ. Applying the curvature correction term for two ellipsoids from Schiller [18], the Derjaguin approximation for electrostatic energy becomes

$$U_e = \frac{\zeta e^{-\kappa D}}{\sqrt{K^I + K^J + 2H^I H^J - 2S^{IJ} cos(2\phi)}}, \tag{3.1.2}$$

with S^{IJ} defined by

$$S^{IJ} = \sqrt{((H^I)^2 - K^I)((H^J)^2 - K^J)}. \tag{3.1.3}$$

When applied to spheres, for which $K = r^{-2}$ and $H = r^{-1}$, equation (3.1.2) matches equation (3.1.1), as expected. When the position vector (x, y, z) describes a point on the surface of an ellipsoid in the particle coordinate system, the Gaussian and mean curvature follow

$$K = \frac{1}{r_x^2 r_y^2 r_z^2 (\frac{x^2}{r_x^4} + \frac{y^2}{r_y^4} + \frac{z^2}{r_z^4})^2}, \tag{3.1.4}$$

$$H = \frac{r_y^2 r_z^2 (r_y^2 + r_z^2)x^2 + r_x^2 r_z^2 (r_x^2 + r_z^2)y^2 + r_x^2 r_y^2 (r_x^2 + r_y^2)z^2}{r_x^2 r_y^2 r_z^2 (\frac{x^2}{r_x^4} + \frac{y^2}{r_y^4} + \frac{z^2}{r_z^4})^{3/2}}. \tag{3.1.5}$$

Relating the distance variables to r_m (which yields $\widetilde{D} = r_m^{-1} D$, $\widetilde{\kappa} = r_m \kappa$, $\widetilde{K} = r_m^2 K$, and $\widetilde{H} = r_m H$) and defining the dimensionless parameter $Z = \zeta r_m / k_B T$ to describe the strength of the electrostatic interactions, the dimensionless form of equation (3.1.2) equals

$$\widetilde{U}_e = \frac{Z e^{-\widetilde{\kappa}\widetilde{D}}}{\sqrt{\widetilde{K}^I + \widetilde{K}^J + 2\widetilde{H}^I \widetilde{H}^J - 2\widetilde{S}^{IJ} cos(2\phi)}}. \tag{3.1.6}$$

Because the minimum separation distance must be calculated numerically, the derivative of equation (3.1.6) must be taken at least partially numerically. For example, consider the repulsive force on particle J given by

$$\widetilde{\mathbf{F}}_e^J = -\widetilde{\nabla}_J \widetilde{U}_e. \tag{3.1.7}$$

Using the definition of gradient, this force is calculated according to

$$\begin{aligned}
\frac{\delta \widetilde{U}_e}{\delta \widetilde{x}_J} &\approx \frac{\widetilde{U}_e\left(\widetilde{x}^J + d, \widetilde{y}^J, \widetilde{z}^I\right) - \widetilde{U}_e\left(\widetilde{x}^J - d, \widetilde{y}^J, \widetilde{z}^J\right)}{2d}, \\
\frac{\delta \widetilde{U}_e}{\delta \widetilde{y}_J} &\approx \frac{\widetilde{U}_e\left(\widetilde{x}^J, \widetilde{y}^J + d, \widetilde{z}^I\right) - \widetilde{U}_e\left(\widetilde{x}^J, \widetilde{y}^J - d, \widetilde{z}^J\right)}{2d}, \\
\frac{\delta \widetilde{U}_e}{\delta \widetilde{z}_J} &\approx \frac{\widetilde{U}_e\left(\widetilde{x}^J, \widetilde{y}^J, \widetilde{z}^I + d\right) - \widetilde{U}_e\left(\widetilde{x}^J, \widetilde{y}^J, \widetilde{z}^J - d\right)}{2d}.
\end{aligned} \tag{3.1.8}$$

As with the numerical calculation of force and torque, the coordinate space in which the result is defined depends on axes on which the particle position is varied. In this work, the particle position is varied in lab space, and thus the resulting torque is transformed from lab space to particle J space to achieve the final result.

Direct numerical gradient calculation is not the only method for finding the electrostatic force. An alternative method calculates the magnitude and the direction of the force separately. Because the gradient vector lies perpendicular to the particle surface, the line that connects the closest points on the surfaces of two particles must run parallel to the

gradient of both particle at those points. Otherwise, moving a point along the surface in the direction of the gradient would lead to a smaller minimum separation distance. From equation (1.2.1) with $\xi = 1$, the gradient of the surface of an ellipsoidal particle follows

$$\nabla = \left(\frac{2x}{r_x^2}, \frac{2y}{r_y^2}, \frac{2z}{r_z^2} \right), \tag{3.1.9}$$

where (x, y, z) describes a point on the particle surface defined in the particle coordinate system. With the direction of the repulsive force easily determined by this simple calculation, the magnitude can be determined analytically from equation (3.1.4) by taking the negative partial derivative with respect to the minimum separation distance $\widetilde{D}$:

$$|\widetilde{\mathbf{F}}_e| = \frac{Z\widetilde{\kappa} e^{-\widetilde{\kappa}\widetilde{D}}}{\sqrt{\widetilde{K}^I + \widetilde{K}^J + 2\widetilde{H}^I\widetilde{H}^J - 2\widetilde{S}^{IJ} cos(2\phi)}}. \tag{3.1.10}$$

This method produces a near identical yet computationally less expensive result than equation (3.1.8), so all simulations in this report use it.

The torque resulting from the electrostatic repulsion is calculated using the general equation for torque from a force applied on a body along an axis that does not necessarily pass through the center of mass:

$$\tau = \mathbf{r} \times \mathbf{F}. \tag{3.1.11}$$

For example, the torque on particle J equals the cross product between the applied force on the particle ($\widetilde{\mathbf{F}}_e^J$, in particle J space) and the distance vector from the particle center of mass to the numerically calculated point on the particle surface where the force is applied ($\widetilde{\mathbf{r}}_D^J$), according to

$$\widetilde{\tau}_e^J = \widetilde{\mathbf{r}}_D^J \times \widetilde{\mathbf{F}}_e^J. \tag{3.1.12}$$

Figure 3.1 shows the dynamics resulting from equations (3.1.10) and (3.1.12) for two pairs of particles. The force field is plotted over the energy landscape, and the torque field is plotted over the torque magnitude landscape.

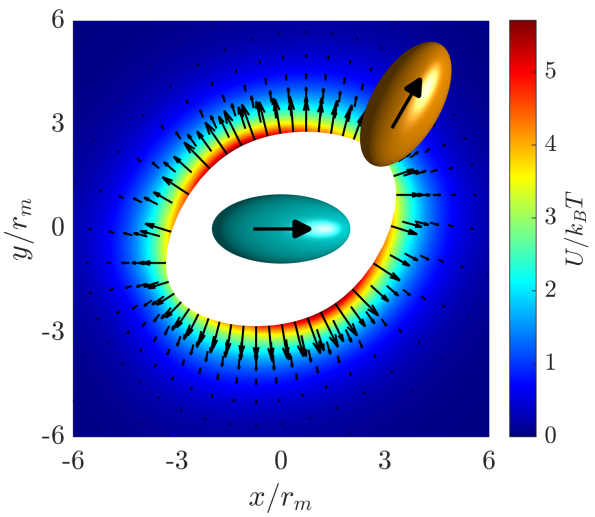

(a) Aspect ratios 2:1:1 and 2:1:1

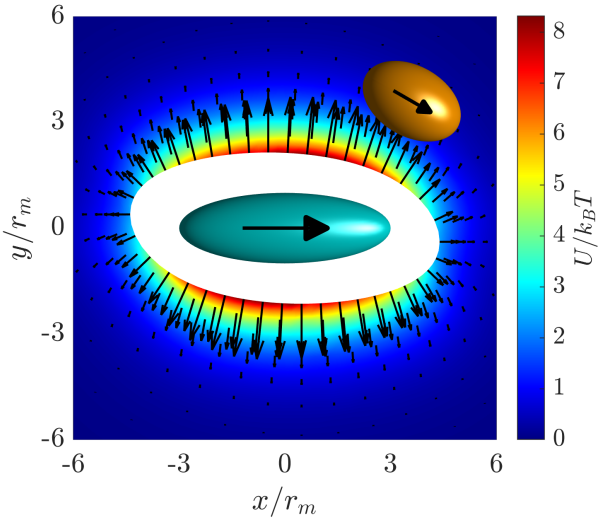

(b) Aspect ratios 3:1:1 and 1.5:1:1

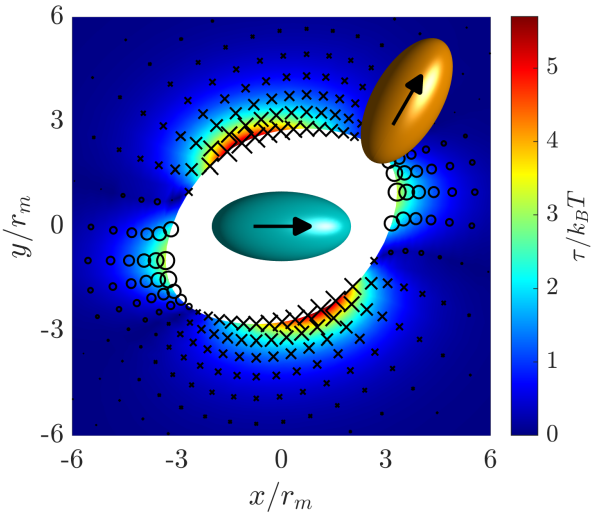

(c) Aspect ratios 2:1:1 and 2:1:1

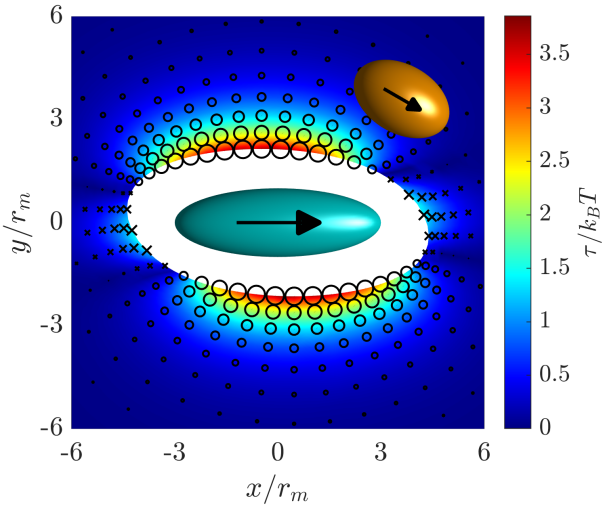

(d) Aspect ratios 3:1:1 and 1.5:1:1

Figure 3.1: Electrostatic (a,c) force and (b,d) torque between particles I and J. For both pairs, magnetizations are $\widetilde{\mathbf{M}}^I = \widetilde{\mathbf{M}}^J = (1, 0, 0)$, $Z = 10$, and $\widetilde{\kappa} = 1$.

3.2 External Magnetic Field

In addition to fields from surrounding particles, magnetic particles also interact with externally applied magnetic fields. In this report, a uniform magnetic field is applied, which exerts no net force on the particles due to its uniformity. However, the external field does exert a torque on the particles, compelling the particles to orient such that their magnetic moments align with the external field. This torque follows $\tau = \mathbf{m} \times \mathbf{H}$, as originally given by equation 2.4.15. Applying this relation to particle-field gives

$$\tau_{df}^{J} = \mathbf{m}^{J} \times \mathbf{A}^{J} \cdot \mathbf{H}^{ext}, \tag{3.2.1}$$

where τ_{df}^{J} is the dipole-field torque on particle J and $\mathbf{H}^{ext}$ is the vector in lab space that describes the strength and direction of the applied external field. Using the relation between magnetic moment and magnetization ($\mathbf{m} = \mu_0 v_p \mathbf{M}$) yields

$$\tau_{df} = \mu_0 v_p \mathbf{M} \times \mathbf{A} \cdot \mathbf{H}^{ext}. \tag{3.2.2}$$

Factoring out the magnitude of the magnetic moment and the external field, and defining the variable ($\widetilde{\tau}_{df}$) in the manner that (1.1.5) suggests, equation (3.2.2) is represented in dimensionless form as

$$\widetilde{\tau}_{df}^{J} = \alpha \cdot \widetilde{\mathbf{M}}^{J} \times \mathbf{A}^{J} \cdot \widetilde{\mathbf{H}}^{ext}, \tag{3.2.3}$$

where the particle-field interaction parameter α is defined by

$$\alpha \equiv \frac{H^0 \mu_0 v_p M}{k_B T}. \tag{3.2.4}$$

Once again, it becomes useful to relate the particle-field interaction parameter for an ellipsoid to that of a sphere with radius r_m. Using equation (2.1.13) gives

$$\alpha_e = \widetilde{r}_x \widetilde{r}_y \widetilde{r}_z \alpha_s. \tag{3.2.5}$$

3.3 Langevin Equation

The Langevin equation describes the motion of particles when subjected to a combination of deterministic and stochastic influences. This differential equation describes a variety of phenomena, including Brownian motion. A form of the Langevin equation based on derivations in Zhao [16] relates the various forces and torques considered in this report:

$$\begin{pmatrix} \mathbf{0} \\ \mathbf{0} \end{pmatrix} = \begin{pmatrix} \mathbf{F}_h \\ \tau_h \end{pmatrix} + \begin{pmatrix} \mathbf{F}_{dd} \\ \tau_{dd} \end{pmatrix} + \begin{pmatrix} \mathbf{F}_{df} \\ \tau_{df} \end{pmatrix} + \begin{pmatrix} \mathbf{F}_e \\ \tau_e \end{pmatrix} + \begin{pmatrix} \mathbf{F}_B \\ \tau_B \end{pmatrix}, \tag{3.3.1}$$

where "$_h$" refers hydrodynamic effects, "$_{dd}$" refers to dipole-dipole interactions, "$_{df}$" refers to dipole-field interactions, "$_e$" refers to electrostatic interactions, and "$_B$" refers to Brownian dynamics. Based on Brenner [19], the inverse of the grand mobility matrix $\mathcal{M}$ relates the force and torque on a particle to the resulting particle movement according to

$$\begin{pmatrix} \mathbf{F} \\ \tau \end{pmatrix} = -\mathcal{M}^{-1} \cdot \begin{pmatrix} \mathbf{u} - \mathbf{u}^{\infty} \\ \omega - \omega^{\infty} \end{pmatrix}, \tag{3.3.2}$$

where $\mathbf{u}$ is the translational velocity and ω is the angular velocity of the particle due to force $\mathbf{F}$ and torque τ, and $\mathbf{u}^{\infty}$ and ω^{∞} describe the flow field of the carrier fluid. Decomposing

the velocity terms into their derivative form and assuming a quiescent carrier fluid yields

$$\begin{pmatrix}\mathbf{F}\\ \tau\end{pmatrix} = -\frac{\mathcal{M}^{-1}}{\Delta t}\cdot\begin{pmatrix}\Delta\mathbf{x}\\ \Delta\mathbf{\Phi}\end{pmatrix}, \tag{3.3.3}$$

where Δt is the time step, $\Delta\mathbf{x}$ is the change in position, and $\Delta\mathbf{\Phi}$ is the change in orientation.

From Brenner [19] and Swan [20], assuming no coupling between translational and rotational motion, the grand mobility matrix for ellipsoidal particles equals

$$\mathcal{M} = \begin{pmatrix}\mathbf{K}^{-1} & 0\\ 0 & \mathbf{\Omega}^{-1}\end{pmatrix}, \tag{3.3.4}$$

where $\mathbf{K}$ is the translational resistance dyadic given by

$$\mathbf{K} = 16\pi\mu\left[\frac{1}{X+{r_x}^2L^{r^x}(\infty)}\mathbf{e_x}\mathbf{e_x} + \frac{1}{X+{r_y}^2L^{r^y}(\infty)}\mathbf{e_y}\mathbf{e_y} + \frac{1}{X+{r_z}^2L^{r^z}(\infty)}\mathbf{e_z}\mathbf{e_z}\right], \tag{3.3.5}$$

$\mathbf{\Omega}$ is the rotational resistance dyadic given by

$$\mathbf{\Omega} = \frac{16\pi}{3}\mu\left[\frac{{r_y}^2+{r_z}^2}{{r_y}^2L^{r^x}(\infty)+{r_z}^2L^{r^x}(\infty)}\mathbf{e_x}\mathbf{e_x} + \frac{{r_x}^2+{r_z}^2}{{r_x}^2L^{r^y}(\infty)+{r_z}^2L^{r^y}(\infty)}\mathbf{e_y}\mathbf{e_y} + \frac{{r_x}^2+{r_y}^2}{{r_x}^2L^{r^z}(\infty)+{r_y}^2L^{r^z}(\infty)}\mathbf{e_z}\mathbf{e_z}\right], \tag{3.3.6}$$

and μ is the dynamic viscosity of the carrier fluid. The function L_i is the shape parameter function in direction i as defined by equation (2.1.7), and X is defined by

$$X = \int_0^\infty \frac{1}{\sqrt{\left(\alpha+r_x^2\right)\left(\alpha+r_y^2\right)\left(\alpha+r_z^2\right)}}d\alpha. \tag{3.3.7}$$

Applying equation (3.3.3) to the hydrodynamics and Brownian motion terms in equation (3.3.1) and solving for the velocity of the particle yields

$$\begin{pmatrix}\mathbf{0}\\ \mathbf{0}\end{pmatrix} = -\frac{\mathcal{M}^{-1}}{\Delta t}\cdot\begin{pmatrix}\Delta\mathbf{x}\\ \Delta\mathbf{\Phi}\end{pmatrix} + \begin{pmatrix}\mathbf{F}_{dd}\\ \tau_{dd}\end{pmatrix} + \begin{pmatrix}\mathbf{F}_{df}\\ \tau_{df}\end{pmatrix} + \begin{pmatrix}\mathbf{F}_{e}\\ \tau_{e}\end{pmatrix} - \frac{\mathcal{M}^{-1}}{\Delta t}\cdot\begin{pmatrix}\Delta\mathbf{x}_B\\ \Delta\mathbf{\Phi}_B\end{pmatrix},$$

$$\begin{pmatrix}\Delta\mathbf{x}\\ \Delta\mathbf{\Phi}\end{pmatrix} = \Delta t\mathcal{M}\begin{pmatrix}\mathbf{F}_{dd}\\ \tau_{dd}\end{pmatrix} + \Delta t\mathcal{M}\begin{pmatrix}\mathbf{F}_{df}\\ \tau_{df}\end{pmatrix} + \Delta t\mathcal{M}\begin{pmatrix}\mathbf{F}_{e}\\ \tau_{e}\end{pmatrix} - \begin{pmatrix}\Delta\mathbf{x}_B\\ \Delta\mathbf{\Phi}_B\end{pmatrix}, \tag{3.3.8}$$

where $\Delta\mathbf{x}$ is the change in position and $\Delta\mathbf{\Phi}$ is the change in orientation of the particle during time step Δt, and $\Delta\mathbf{x}_B$ is the random change in position and $\Delta\mathbf{\Phi}_B$ is the random change in orientation due to Brownian movement of the particle.

Brownian motion results from the random collisions of vibrating particles in a fluid. Due to the random nature of these collisions, a Gaussian distribution of randomly generated vectors with a mean $\mu = 0$ can simulate Brownian motion. For translational motion, the distribution of $\Delta\mathbf{x}$ vectors must have a variance (σ_x^2) following

$$\sigma_x^2 = 2\mathbf{D}_x\Delta t, \tag{3.3.9}$$

where $\mathbf{D}_x$ is the translational diffusivity tensor of the particle in the fluid. The set of $\Delta\mathbf{\Phi}$ vectors must follow the same rules, with

$$\sigma_r^2 = 2\mathbf{D}_r\Delta t, \tag{3.3.10}$$

where σ_r^2 is the rotational variance and $\mathbf{D}_r$ is the rotational diffusivity tensor of the particle in the fluid. To numerically produce a Gaussian distribution, the Modified Box-Muller transform proves useful. Given two random values (C_1 and C_2) between 0 and 1, this algorithm numerically generates a normal distribution with a unit standard deviation and a mean $\mu = 0$. This operation is defined by

$$BM = \sqrt{-2ln(C_1)} \cdot cos(2\pi C_2). \tag{3.3.11}$$

To adjust the standard deviation, equation (3.3.11) can be multiplied by the square root of the variance. Applying this principle in equation (3.3.8) yields

$$\begin{pmatrix}\Delta\mathbf{x}\\ \Delta\mathbf{\Phi}\end{pmatrix} = \Delta t\mathcal{M}\begin{pmatrix}\mathbf{F}_{dd}\\ \tau_{dd}\end{pmatrix} + \Delta t\mathcal{M}\begin{pmatrix}\mathbf{F}_{df}\\ \tau_{df}\end{pmatrix} + \Delta t\mathcal{M}\begin{pmatrix}\mathbf{F}_{e}\\ \tau_{e}\end{pmatrix} - \begin{pmatrix}\sqrt{2\mathbf{D}_x\Delta t}(BM)\\ \sqrt{2\mathbf{D}_r\Delta t}(BM)\end{pmatrix}. \tag{3.3.12}$$

The diffusivity tensors $\mathbf{D}_x$ and $\mathbf{D}_r$ depend on the properties of both the fluid and the particle. In general, according to the Einstein relation of kinetic theory, the diffusivity of a sphere in a viscous fluid follows

$$\mathbf{D}_x^{sph} = \mathbf{I}\frac{k_BT}{6\pi\mu r}, \tag{3.3.13}$$

$$\mathbf{D}_r^{sph} = \mathbf{I}\frac{k_BT}{8\pi\mu r^3}, \tag{3.3.14}$$

where $\mathbf{I}$ is the identity matrix. Note that because of the perfect symmetry of spheres, all three particle axes have the same diffusivity, which manifests in a symmetric diffusivity tensor. To find the $\mathbf{D}_x$ and $\mathbf{D}_r$ for ellipsoids, the asymmetry of the particles must be considered. Noting that $\mathbf{K} = 6\pi\mu r\mathbf{I}$ and $\mathbf{\Omega} = 8\pi\mu r^3\mathbf{I}$ for spherical particles,

$$\mathbf{D}_x = k_BT\mathbf{K}^{-1}, \tag{3.3.15}$$

$$\mathbf{D}_r = k_BT\mathbf{\Omega}^{-1}. \tag{3.3.16}$$

Substituting these equations and the the definition of $\mathcal{M}$ into equation (3.3.12), then simplifying with dimensionless variables, and finally implementing $\mathbf{\Psi}$ so that quaternions describe orientation (see Appendix F), yields

$$\begin{pmatrix}\Delta\widetilde{\mathbf{x}}\\ \Delta\mathbf{q}\end{pmatrix} = \begin{pmatrix}\mathbf{I}\\ \mathbf{\Psi}\end{pmatrix}\left[\Delta\widetilde{t}\widetilde{\mathcal{M}}\begin{pmatrix}\widetilde{\mathbf{F}}_{dd}\\ \widetilde{\tau}_{dd}\end{pmatrix} + \Delta\widetilde{t}\widetilde{\mathcal{M}}\begin{pmatrix}\widetilde{\mathbf{F}}_{df}\\ \widetilde{\tau}_{df}\end{pmatrix} + \Delta\widetilde{t}\widetilde{\mathcal{M}}\begin{pmatrix}\widetilde{\mathbf{F}}_{e}\\ \widetilde{\tau}_{e}\end{pmatrix} - \begin{pmatrix}\sqrt{\frac{2}{3}\Delta\widetilde{t}\widetilde{\Omega}_{min}\widetilde{\mathbf{K}}^{-1}}(BM)\\ \sqrt{2\Delta\widetilde{t}\widetilde{\Omega}_{min}\widetilde{\mathbf{\Omega}}^{-1}}(BM)\end{pmatrix}\right], \tag{3.3.17}$$

where $\widetilde{\mathcal{M}}$ is the dimensionless mobility matrix given by

$$\widetilde{\mathcal{M}} = \begin{pmatrix} \frac{1}{3}\widetilde{\Omega}_{min}\widetilde{\mathbf{K}}^{-1} & 0 \\ 0 & \widetilde{\Omega}_{min}\widetilde{\mathbf{\Omega}}^{-1} \end{pmatrix}. \tag{3.3.18}$$

Equations (3.3.17) and (3.3.18) successfully relates the dimensionless forces and torques previously described in this report to a change in particle position and quaternion.

Chapter 4

Simulation Results

4.1 Trajectory Projections

To simulate the motion of two interacting particles, the change in position and orientation is calculated and integrated over many successive small time steps. To keep the particles in relatively close proximity, a periodic boundary condition is applied that contains the particles inside a defined box by relocating the particles to the one side of the box when they leave through the opposing side. To prevent this boundary from separating actively interacting particles, the boundary condition is only applied if the interparticle separation distance is greater than half the box diameter. The dimensionless time step $\Delta\widetilde{t}$ is scaled according to the strength of the interaction and interparticle separation distance, with 10^{-2} set as an upper limit. If particle overlap occurs, the simulation step is rejected and recalculated with a fresh set of random Brownian vectors.

The results of these simulations for several types of interactions are shown in Figures 4.1, Figure 4.2, and Figure 4.3. These figures represent the results through projecting the density of relative positions onto the coordinate planes of the central particle. In other words, areas of high color density indicate that the particle not shown in the figure tends to be in the corresponding three-dimensional position relative to the particle in the center. For all figures except the first, the two particles are identical, and so only the projection of one particle is shown. All simulations use a dimensionless Debye length $\widetilde{\kappa} = 32.9$ and a electrostatic energy parameter $Z = 1268$. Each of the individual figures represents ten successive individual simulations with random initial positions and orientations, which ensures greater exploration of the possible relative configurations.

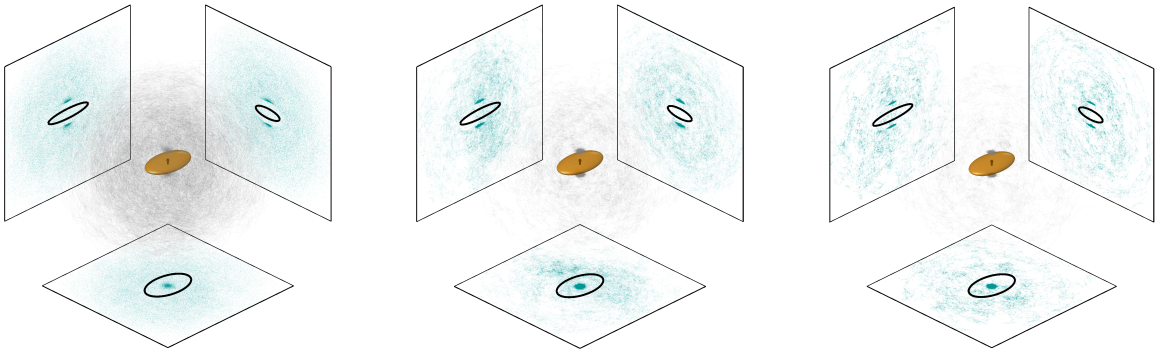

(a) $\beta = 20$ (b) $\beta = 40$ (c) $\beta = 60$

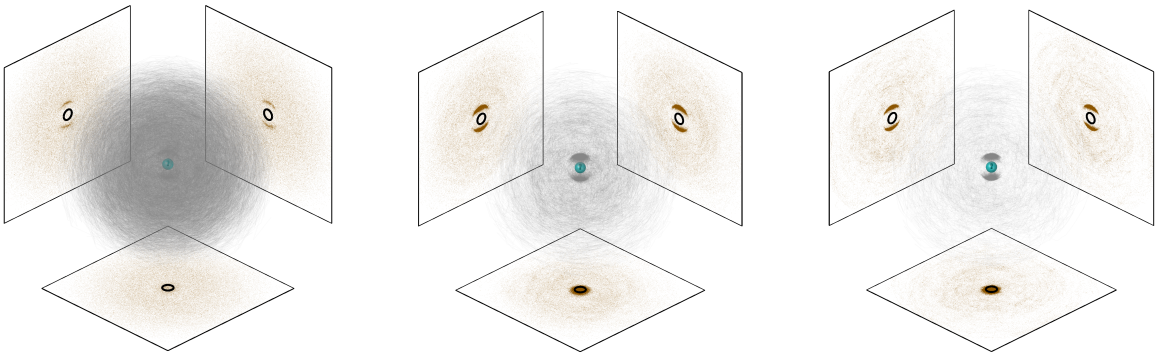

(d) $\beta = 20$ (e) $\beta = 40$ (f) $\beta = 60$

Figure 4.1: Simulations of binary particles with varied dipolar interaction strengths, plotted in (a,b,c) I space and (d,e,f) J space. Aspect ratios 1:3:5 for particle I and 1:3:5 for particle J, magnetizations $\widetilde{\mathbf{M}}^I = \widetilde{\mathbf{M}}^J = (0, 0, 1)$, $\alpha = 20$, and $\Omega = 1$.

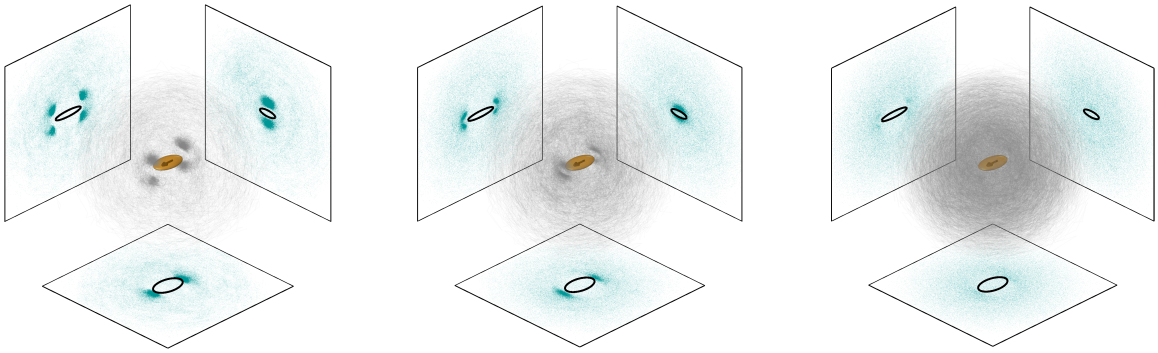

(a) $\Omega = 1$ (b) $\Omega = 3$ (c) $\Omega = 10$

Figure 4.2: Simulations of tri-axial particles with varied external field frequencies. Aspect ratio 1:3:5 for both particles, magnetizations $\widetilde{\mathbf{M}}^I = \widetilde{\mathbf{M}}^J = (1, 0, 0)$, $\alpha = 20$, and $\beta = 100$.

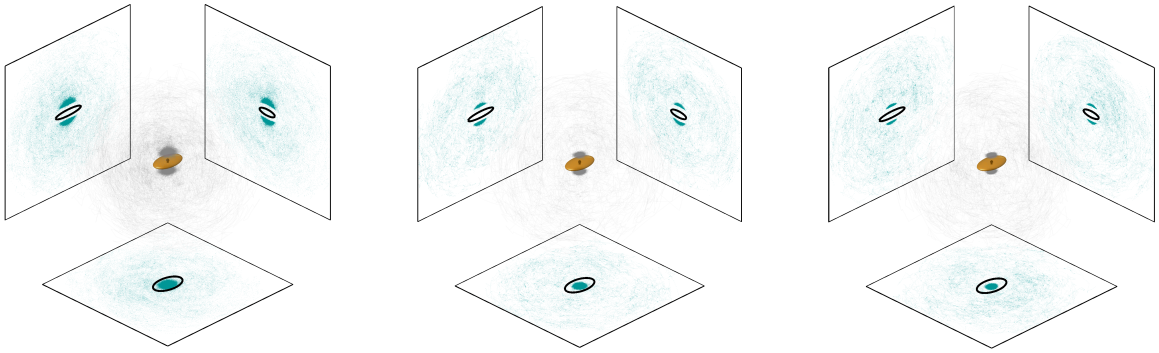

(a) $\beta = 20$, $\widetilde{\mathbf{M}}^I = (0, 0, 1)$ (b) $\beta = 40$, $\widetilde{\mathbf{M}}^I = (0, 0, 1)$ (c) $\beta = 60$, $\widetilde{\mathbf{M}}^I = (0, 0, 1)$

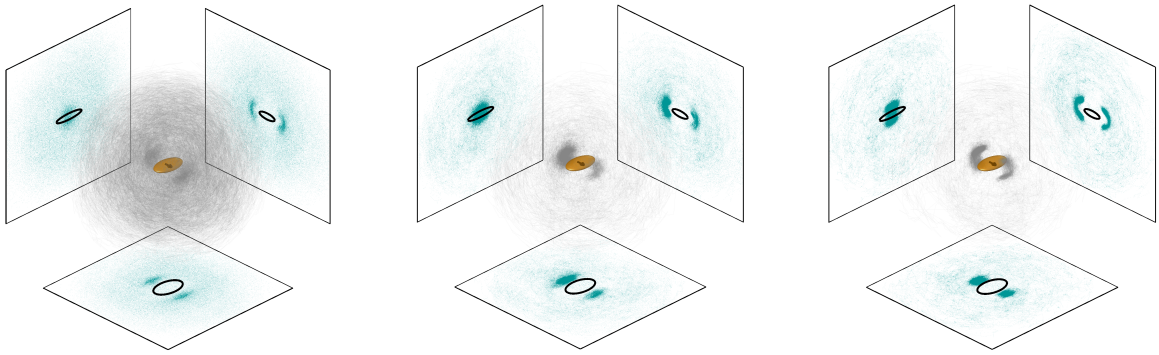

(d) $\beta = 40$, $\widetilde{\mathbf{M}}^I = (0, 1, 0)$ (e) $\beta = 60$, $\widetilde{\mathbf{M}}^I = (0, 1, 0)$ (f) $\beta = 80$, $\widetilde{\mathbf{M}}^I = (0, 1, 0)$

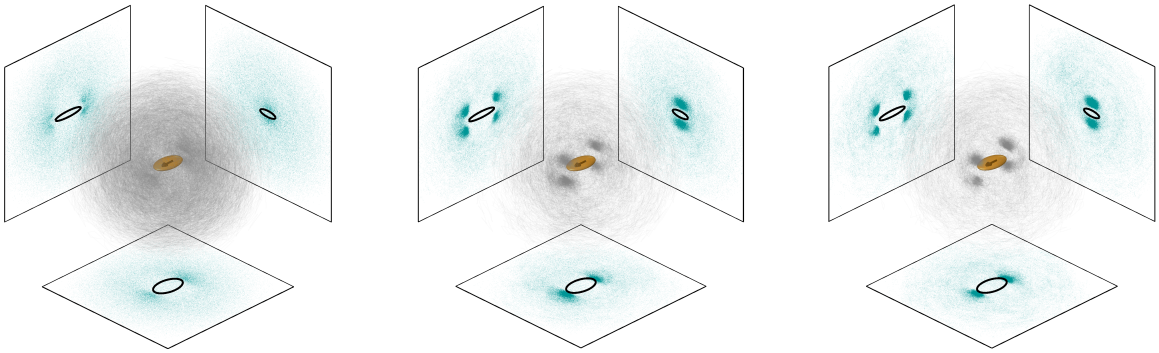

(g) $\beta = 60$,$\widetilde{\mathbf{M}}^I = (1, 0, 0)$ (h) $\beta = 80$,$\widetilde{\mathbf{M}}^I = (1, 0, 0)$ (i) $\beta = 100$,$\widetilde{\mathbf{M}}^I = (1, 0, 0)$

Figure 4.3: Simulations of tri-axial particles with varied magnetizations and dipolar interaction strengths. Aspect ratio 1:3:5 for both particles, $\alpha = 20$, and $\Omega = 1$.

4.2 Mean Squared Displacement

Mean squared displacement (MSD) analysis offers itself as a convenient method for verifying the validity of Brownian dynamics simulations. As its name implies, MSD measures the average squared dislocation of a particle from its initial position. For any random walker, such as a particle experiencing Brownian motion, this value should be proportional to the particle's translational diffusivity. Any discrepancy in this correlation indicates an error in the simulation. According to Medved [21], this relation follows

$$MSD_i = 2D_{x,i}\Delta t, \tag{4.2.1}$$

where MSD_i is the mean squared displacement in coordinate direction i, $D_{x,i}$ is translational diffusivity in coordinate direction i, and Δt is the lag time between the initial and final positions. Rearranging this yields

$$\frac{MSD_i}{\Delta t} = 2D_{x,i}, \tag{4.2.2}$$

which, given the initial condition that the $MSD_i = 0$ at $\Delta t = 0$, implies that the slope of MSD_i versus Δt equals a constant multiple of the diffusivity. Thus, to verify the validity of a given simulation, the average slope of MSD_i versus Δt is calculated using a linear regression. If the simulation is accurate, the slope will approach $2D_{x,i}$ as the number of averaged simulations increases.

For each of the three coordinate directions aligning with semi-axes of an ellipsoidal particle, $D_{x,i}$ can be calculated from equation (3.3.15). For any coordinate direction, MSD_i can be calculated with

$$MSD_i \equiv \langle |x_i(t_0 + \Delta t) - x_i(t_0)|^2 \rangle, \tag{4.2.3}$$

where x_i is the position of the particle along the i axis, t_0 is the initial time, and $\langle\rangle$ denotes the mean across several simulations. The quantity under the square is often abbreviated as $|\Delta x_i|^2$ and interpreted as the change in x_i across Δt. Equation (4.2.3) can be summed along each axis to yield the total MSD in higher dimensions. This also applies to equation (4.2.2), yielding a relation between the total MSD and the diffusivity. In summary, the calculation and expected result for n dimensions follows

$$\frac{MSD}{\Delta t} = \frac{\langle \sum_i^n |\Delta x_i|^2 \rangle}{\Delta t} = 2\sum_i^n D_{x,i}. \tag{4.2.4}$$

Putting equation (4.2.2) in dimensionless form and rearranging to solve for equation (4.2.4) in dimensionless form yields

$$r_m^2 \widetilde{MSD}_i \left(\frac{D_{r,max}}{\Delta \widetilde{t}} \right) = 2D_{x,i},$$

$$\frac{\widetilde{MSD}_i}{\Delta\widetilde{t}} = \frac{2}{r_m^2}\left(\frac{k_BT}{K_i}\right)\left(\frac{\Omega_{min}}{k_BT}\right),$$

$$\frac{\widetilde{MSD}_i}{\Delta\widetilde{t}} = \frac{2}{r_m^2}\left(\frac{16\pi\mu r_m^3\widetilde{\Omega}_{min}}{3\cdot 16\pi\mu r_m\widetilde{K}_i}\right),$$

$$\frac{\widetilde{MSD}_i}{\Delta\widetilde{t}} = \frac{2}{3}\left(\frac{\widetilde{\Omega}_{min}}{\widetilde{K}_i}\right), \tag{4.2.5}$$

where $\widetilde{K}_i$ is the component of $\widetilde{\mathbf{K}}$ in the i direction. Applying this relation to multiple dimensions gives

$$\frac{\widetilde{MSD}}{\Delta\widetilde{t}} = \frac{2}{3}\widetilde{\Omega}_{min}\sum_i^n \frac{1}{\widetilde{K}_i}. \tag{4.2.6}$$

Figure 4.4 presents the mean squared displacement analysis for various particles and conditions. All calculations use the mean of 10^4 simulations, each with $4*10^2$ time steps and $\Delta\widetilde{t} = 10^{-2}$. For each case, the expected slope of $\widetilde{MSD}$ versus $\Delta\widetilde{t}$ as predicted by equation (4.2.6) is compared to the simulated slope as the number of simulations increases. The theoretical and simulation results match well.

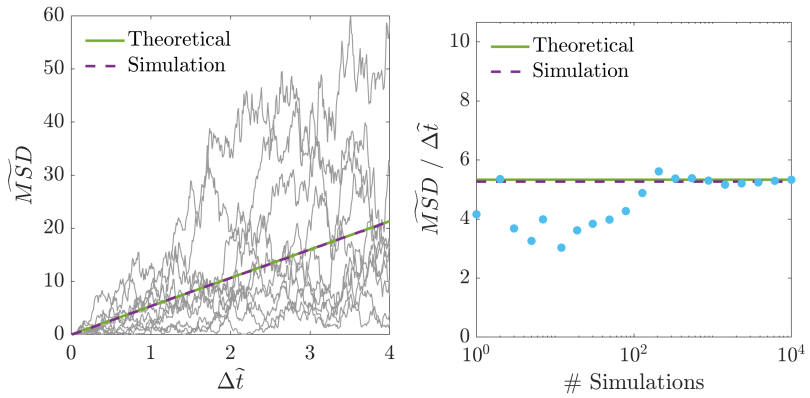

(a) Spherical particle moving in 2D space.

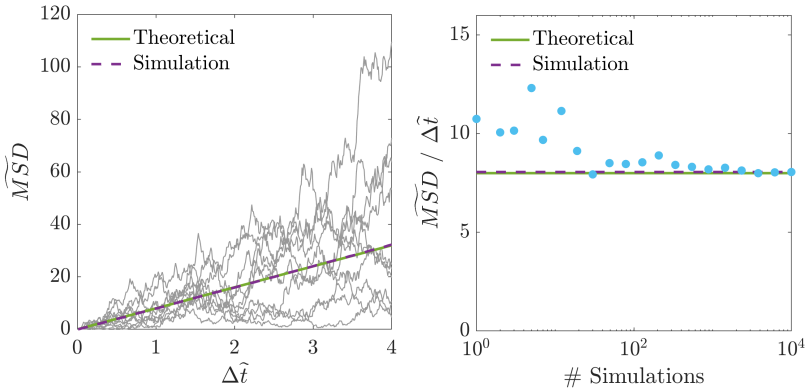

(b) Spherical particle moving in 3D space.

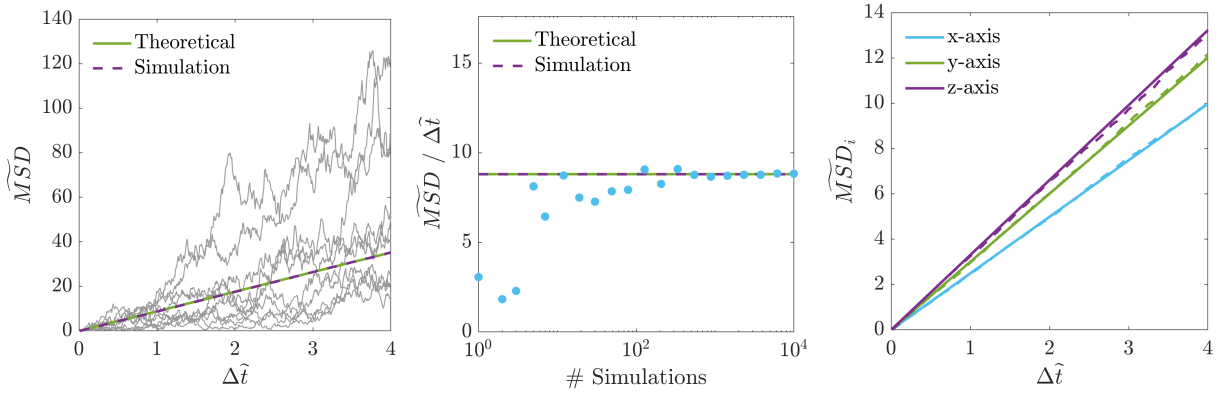

(c) Tri-axial particle moving in 3D space.

Figure 4.4: Mean squared displacement analysis for spherical and tri-axial particles in two and three dimensions. The first panel in each subfigure reports the squared displacements for several simulations along with the theoretical and simulated mean. The second panel shows how the simulated $\widetilde{MSD}/\Delta\widetilde{t}$ converges on the theoretical value as the number of averaged simulations increases. The third panel (only in subfigure c) gives the theoretical and simulated $\widetilde{MSD}_i$ for each axis.

4.3 Rotational Mean Squared Displacement

In a similar manner as MSD, rotational mean squared displacement ($RMSD$) can verify the validity of the rotational aspect of Brownian dynamics simulations. However, unlike MSD, the angular displacement of a particle from its initial orientation has an natural limit, (π radians). Thus, many methods of calculating and analyzing $RMSD$ have been developed. This report considers two methods, one "bounded" analysis and one "unbounded" analysis. The bounded result approaches a limit as the simulation time increases, and the analysis relies on how quickly this limit is reached. On the other hand, the unbounded calculation mirrors the MSD method, and the analysis relies on the slope of the result versus $\Delta\widetilde{t}$.

The $RMSD_b$ (bounded) analysis as described by Jain [22] is defined according to

$$RMSD_b = \langle|\widehat{\mathbf{r}}(t_0 + \Delta t) - \widehat{\mathbf{r}}(t_0)|^2\rangle, \tag{4.3.1}$$

where $\widehat{\mathbf{r}}$ is any unit vector with a fixed orientation with respect to the particle. When averaged across many simulations, the result should match the theoretical model given by

$$RMSD_b = 2(1 - e^{-2D_r\Delta t}). \tag{4.3.2}$$

Note that since this equation depends on D_r and the three diagonal components of $\mathbf{D_r}$ only equal each other for spherical particles, this analysis is only suitable for spherical particles. Dimensionless equation (4.3.2) equals

$$RMSD_b = 2(1 - e^{-2\Delta\widetilde{t}}). \tag{4.3.3}$$

The $RMSD_u$ (unbounded) analysis as described by Hunter [23] relies on a change in orientation vector $\mathbf{\Phi}$ calculated according to

$$\mathbf{\Phi}(\Delta t) = \int_0^{\Delta t} \omega(t')dt' \tag{4.3.4}$$

where ω is angular velocity. Using this definitions, $RMSD_u$ is defined according to

$$RMSD_u = \langle|\mathbf{\Phi}(t_0 + \Delta t) - \mathbf{\Phi}(t_0)|^2\rangle. \tag{4.3.5}$$

When rotating in n dimensions, the slope of $RMSD_u$ versus $\Delta\widetilde{t}$ should equal

$$\frac{RMSD_u}{\Delta t} = 2\sum_i^n D_{r,i}. \tag{4.3.6}$$

The dimensionless form of this equation equals

$$\frac{RMSD_u}{\Delta\widetilde{t}} = 2\widetilde{\Omega}_{min}\sum_i^n \frac{1}{\widetilde{\Omega}_i}. \tag{4.3.7}$$

Figures 4.5 and 4.6 display the results of the bounded and unbounded $RMSD$ calculations, respectively. As with the MSD simulations, all calculations use the mean of 10^4 simulations, each with $4 * 10^2$ time steps with a time step of 10^{-2}. The bounded result is compared to equation (4.3.3), and the slope of the unbounded calculation is compared to equation (4.3.7). The theoretical and simulation results match well.

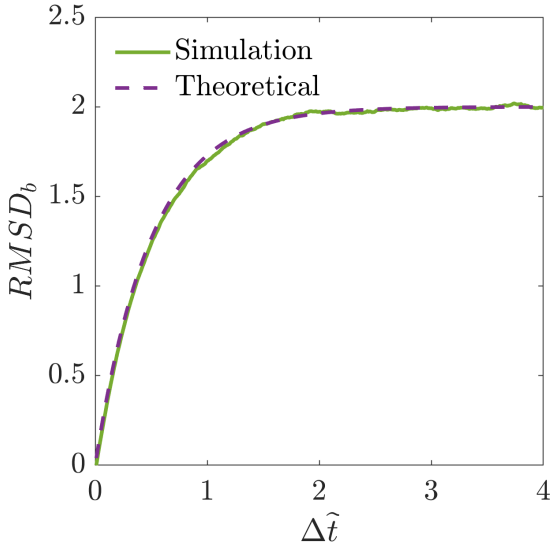

Figure 4.5: Bounded rotational mean squared displacement, based on Jain [22].

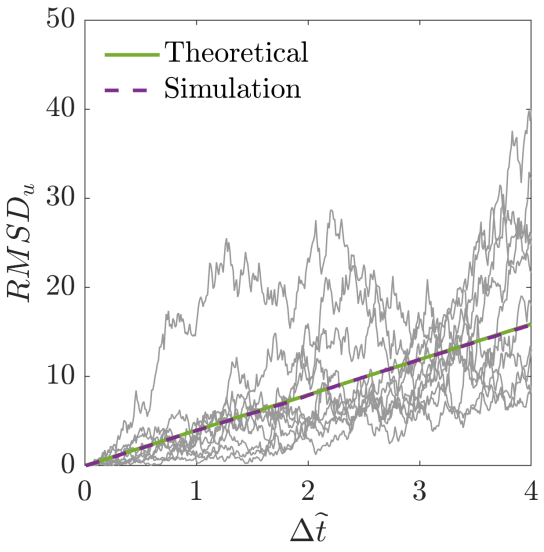

(a) $RMSD_u$ for several simulations and the theoretical and simulated mean.

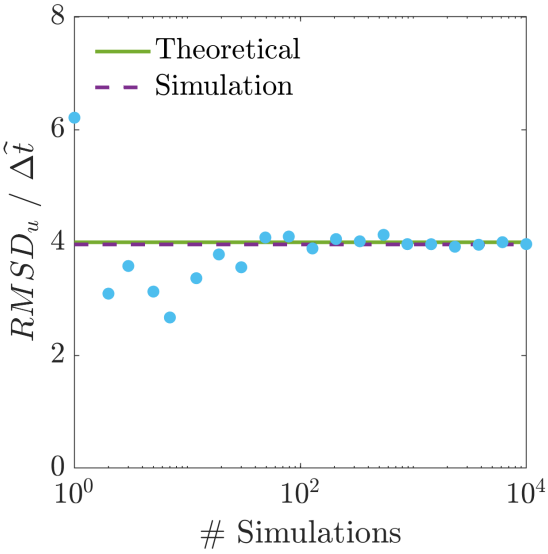

(b) Convergence of $RMSD_u/\Delta\widetilde{t}$ with number of averaged simulations.

Figure 4.6: Unbounded rotational mean squared displacement, based on Hunter [23].

Chapter 5

Conclusion

This work derived an analytical model for the dipolar interaction of magnetic ellipsoids and verified the dynamics through both numerical calculations and comparison with the established point-dipole model. Then, the model was applied in Brownian dynamics simulations along with a rotating external magnetic field and an electrostatic potential that accounts for particle curvature at the point of interaction. Next, several simulations were performed of tri-axial and binary particles in various conditions, revealing how each parameter affects the particle interactions. Finally, the validity of the simulations were confirmed using both translational and rotational mean squared displacement analysis.

In the future, the simulation techniques and code derived in this work will be applied to simulations of dense particle suspensions, in which multiple particles interact simultaneously. Because the behavior of these suspensions is experimentally known, this will verify the validity of the simulation method, lending credence to any simulation-based predictions about the behavior of possible nanorobot designs.

Bibliography

[1] G. Giri, Y. Maddahi, and K. Zareinia, "A brief review on challenges in design and development of nanorobots for medical applications," *Applied Sciences*, vol. 11, no. 21, p. 10385, 2021.

[2] Y. Kim, H. Yuk, R. Zhao, S. A. Chester, and X. Zhao, "Printing ferromagnetic domains for untethered fast-transforming soft materials," *Nature*, vol. 558, no. 7709, pp. 274–279, 2018.

[3] S. Kim, S. Lee, J. Lee, B. J. Nelson, L. Zhang, and H. Choi, "Fabrication and manipulation of ciliary microrobots with non-reciprocal magnetic actuation," *Scientific reports*, vol. 6, no. 1, p. 30713, 2016.

[4] J. Giltinan, V. Sridhar, U. Bozuyuk, D. Sheehan, and M. Sitti, "3d microprinting of iron platinum nanoparticle-based magnetic mobile microrobots," *Advanced Intelligent Systems*, vol. 3, no. 1, p. 2000204, 2021.

[5] M. Wehner, R. L. Truby, D. J. Fitzgerald, B. Mosadegh, G. M. Whitesides, J. A. Lewis, and R. J. Wood, "An integrated design and fabrication strategy for entirely soft, autonomous robots," *nature*, vol. 536, no. 7617, pp. 451–455, 2016.

[6] S. Mohanty, J. Zhang, J. M. McNeill, T. Kuenen, F. P. Linde, J. Rouwkema, and S. Misra, "Acoustically-actuated bubble-powered rotational micro-propellers," *Sensors and Actuators B: Chemical*, vol. 347, p. 130589, 2021.

[7] C. C. Alcântara, S. Kim, S. Lee, B. Jang, P. Thakolkaran, J.-Y. Kim, H. Choi, B. J. Nelson, and S. Pané, "3d fabrication of fully iron magnetic microrobots," *Small*, vol. 15, no. 16, p. 1805006, 2019.

[8] R. Cheng, L. Zhu, W. Huang, L. Mao, and Y. Zhao, "Reconfiguring ferromagnetic microrod chains by alternating two orthogonal magnetic fields," *Journal of Physics: Condensed Matter*, vol. 30, no. 31, p. 315101, 2018.

[9] J. Faraudo, J. S. Andreu, C. Calero, and J. Camacho, "Predicting the self-assembly of superparamagnetic colloids under magnetic fields," *Advanced Functional Materials*, vol. 26, no. 22, pp. 3837–3858, 2016.

[10] B. W. Kwaadgras, R. Van Roij, and M. Dijkstra, "Self-consistent electric field-induced dipole interaction of colloidal spheres, cubes, rods, and dumbbells," *The Journal of Chemical Physics*, vol. 140, no. 15, p. 154901, 2014.

[11] E. M. Purcell, "Life at low reynolds number," *American journal of physics*, vol. 45, no. 1, pp. 3–11, 1977.

[12] D. J. Evans, "On the representatation of orientation space," *Molecular physics*, vol. 34, no. 2, pp. 317–325, 1977.

[13] O. M. O'Reilly, *Intermediate Dynamics for Engineers: Newton-Euler and Lagrangian Mechanics*. Cambridge University Press, 2020.

[14] S. Delong, F. Balboa Usabiaga, and A. Donev, "Brownian dynamics of confined rigid bodies," *The Journal of chemical physics*, vol. 143, no. 14, p. 144107, 2015.

[15] B. F. Edwards, D. M. Riffe, J.-Y. Ji, and W. A. Booth, "Interactions between uniformly magnetized spheres," *American Journal of Physics*, vol. 85, no. 2, pp. 130–134, 2017.

[16] Z. Zhao and C. Rinaldi, "Magnetization dynamics and energy dissipation of interacting magnetic nanoparticles in alternating magnetic fields with and without a static bias field," *The Journal of Physical Chemistry C*, vol. 122, no. 36, pp. 21018–21030, 2018.

[17] J. N. Israelachvili, *Intermolecular and surface forces*. Academic press, 2011.

[18] P. Schiller, S. Kruger, M. Wahab, and H.-J. Mogel, "Interactions between spheroidal colloidal particles," *Langmuir*, vol. 27, no. 17, pp. 10429–10437, 2011.

[19] H. Brenner, "The stokes resistance of an arbitrary particle—iii: Shear fields," *Chemical Engineering Science*, vol. 19, no. 9, pp. 631–651, 1964.

[20] J. W. Swan and J. F. Brady, "Simulation of hydrodynamically interacting particles near a no-slip boundary," *Physics of Fluids*, vol. 19, no. 11, p. 113306, 2007.

[21] A. Medved, R. Davis, and P. A. Vasquez, "Understanding fluid dynamics from langevin and fokker–planck equations," *Fluids*, vol. 5, no. 1, p. 40, 2020.

[22] R. Jain and K. Sebastian, "Diffusing diffusivity: Rotational diffusion in two and three dimensions," *The Journal of chemical physics*, vol. 146, no. 21, p. 214102, 2017.

[23] G. L. Hunter, K. V. Edmond, M. T. Elsesser, and E. R. Weeks, "Tracking rotational diffusion of colloidal clusters," *Optics express*, vol. 19, no. 18, pp. 17189–17202, 2011.

Chapter 6

Appendices

6.1 Appendix A

Functions with no accents denote functions of extensive variables, and functions accented with a tilde denote functions of dimensionless variables. From equation (2.1.6):

$$G_{ij} = \delta_{ij}\left(L_{r_j}(\xi) - L_{r_j}(\infty)\right) + x_j \frac{\delta L_{r_j}(\xi)}{\delta x_i} \tag{6.1.1}$$

$$G_{ij} = \delta_{ij}\left(L_{r_j}(\xi) - L_{r_j}(\infty)\right) + x_j \left(F_{r_j}(\xi)\frac{\delta \xi}{\delta x_i}\right) \tag{6.1.2}$$

In dimensionless form:

$$\widetilde{G}_{ij} = \delta_{ij}\left(L^{\widetilde{r}^j}\left(\widetilde{\xi}\right) - L^{\widetilde{r}^j}(\infty)\right) + \widetilde{x}_j \left(F^{\widetilde{r}^j}(\widetilde{\xi})\frac{\delta \widetilde{\xi}}{\delta \widetilde{x}_i}\right) \tag{6.1.3}$$

Finding a definition for $\widetilde{\xi}$:

$$\frac{\widetilde{x}^2}{\widetilde{r}_x^2 + \widetilde{\xi}} + \frac{\widetilde{y}^2}{\widetilde{r}_y^2 + \widetilde{\xi}} + \frac{\widetilde{z}^2}{\widetilde{r}_z^2 + \widetilde{\xi}} = 1 \tag{6.1.4}$$

$$\frac{r_m^2\widetilde{x}^2}{r_m^2\widetilde{r}_x^2 + \xi} + \frac{r_m^2\widetilde{y}^2}{r_m^2\widetilde{r}_y^2 + \xi} + \frac{r_m^2\widetilde{z}^2}{r_m^2\widetilde{r}_z^2 + \xi} = 1 \tag{6.1.5}$$

$$\frac{\widetilde{x}^2}{\widetilde{r}_x^2 + \frac{\xi}{r_m^2}} + \frac{\widetilde{y}^2}{\widetilde{r}_y^2 + \frac{\xi}{r_m^2}} + \frac{\widetilde{z}^2}{\widetilde{r}_z^2 + \frac{\xi}{r_m^2}} = 1 \tag{6.1.6}$$

$$\widetilde{\xi} = \frac{\xi}{r_m^2}\ , \quad r_m^2\widetilde{\xi} = \xi \tag{6.1.7}$$

Using this relation to find $\delta\widetilde{\xi}/\delta\widetilde{x}_i$:

$$\frac{\delta\xi}{\delta x_i} = \frac{\delta\left(r_m^2\widetilde{\xi}\right)}{\delta x_i} = r_m^2\frac{\delta\widetilde{\xi}}{\delta\widetilde{x}_i}\frac{\delta\widetilde{x}_i}{\delta x_i} = r_m^2\frac{\delta\widetilde{\xi}}{\delta\widetilde{x}_i}\left(\frac{1}{r_m}\right) = r_m\frac{\delta\widetilde{\xi}}{\delta\widetilde{x}_i} \tag{6.1.8}$$

Substituting equations (2.1.9), (6.1.7), and (6.1.8) into equation (6.1.1):

$$G_{ij} = \delta_{ij}\left(L_{r_j}\left(r_m^2\widetilde{\xi}\right) - L_{r_j}(\infty)\right) + r_m\widetilde{x}_j\left(F_{r_j}(r_m^2\widetilde{\xi})\cdot r_m\frac{\delta\widetilde{\xi}}{\delta\widetilde{x}_i}\right) \tag{6.1.9}$$

Using equation (2.1.8) for F_{r_j}:

$$F^{\widetilde{r}^j}\left(\widetilde{\xi}\right) = \frac{1}{(\widetilde{\xi}+\widetilde{r}_j^2)\sqrt{(\widetilde{\xi}+\widetilde{r}_x^2)(\widetilde{\xi}+\widetilde{r}_y^2)(\widetilde{\xi}+\widetilde{r}_z^2)}} \tag{6.1.10}$$

$$F_{r_j}\left(r_m^2\widetilde{\xi}\right) = \frac{1}{(r_m^2\widetilde{\xi}+r_m^2\widetilde{r}_j^2)\sqrt{(r_m^2\widetilde{\xi}+r_m^2\widetilde{r}_x^2)(r_m^2\widetilde{\xi}+r_m^2\widetilde{r}_y^2)(r_m^2\widetilde{\xi}+r_m^2\widetilde{r}_z^2)}} \tag{6.1.11}$$

$$F_{r_j}\left(r_m^2\widetilde{\xi}\right) = \frac{1}{r_m^5}\frac{1}{(\widetilde{\xi}+\widetilde{r}_j^2)\sqrt{(\widetilde{\xi}+\widetilde{r}_x^2)(\widetilde{\xi}+\widetilde{r}_y^2)(\widetilde{\xi}+\widetilde{r}_z^2)}} \tag{6.1.12}$$

$$F_{r_j}\left(r_m^2\widetilde{\xi}\right) = \frac{1}{r_m^5}F^{\widetilde{r}^j}\left(\widetilde{\xi}\right) \tag{6.1.13}$$

Using equation (2.1.7) for L_{r_j}:

$$L^{\widetilde{r}^j}\left(\widetilde{\xi}\right) = \int_0^{\widetilde{\xi}}\frac{1}{(\alpha+\widetilde{r}_j^2)\sqrt{(\alpha+\widetilde{r}_x^2)(\alpha+\widetilde{r}_y^2)(\alpha+\widetilde{r}_z^2)}}d\alpha \tag{6.1.14}$$

$$L_{r_j}\left(r_m^2\widetilde{\xi}\right) = \int_0^{r_m^2\widetilde{\xi}}\frac{1}{(\alpha+r_m^2\widetilde{r}_j^2)\sqrt{(\alpha+r_m^2\widetilde{r}_x^2)(\alpha+r_m^2\widetilde{r}_y^2)(\alpha+r_m^2\widetilde{r}_z^2)}}d\alpha \tag{6.1.15}$$

$$\gamma = \frac{\alpha}{r_m^2}\ ,\quad d\gamma = \frac{d\alpha}{r_m^2} \tag{6.1.16}$$

$$L_{r_j}\left(r_m^2\widetilde{\xi}\right) = \int_0^{\widetilde{\xi}}\frac{r_m^2}{(r_m^2\gamma+r_m^2\widetilde{r}_j^2)\sqrt{(r_m^2\gamma+r_m^2\widetilde{r}_x^2)(r_m^2\gamma+r_m^2\widetilde{r}_y^2)(r_m^2\gamma+r_m^2\widetilde{r}_z^2)}}d\gamma \tag{6.1.17}$$

$$L_{r_j}\left(r_m^2\widetilde{\xi}\right) = \int_0^{\widetilde{\xi}}\frac{r_m^2}{r_m^5(\gamma+\widetilde{r}_j^2)\sqrt{(\gamma+\widetilde{r}_x^2)(\gamma+\widetilde{r}_y^2)(\gamma+\widetilde{r}_z^2)}}d\gamma \tag{6.1.18}$$

$$L_{r_j}\left(r_m^2\widetilde{\xi}\right) = \frac{1}{r_m^3}\int_0^{\widetilde{\xi}}\frac{1}{(\gamma+\widetilde{r}_j^2)\sqrt{(\gamma+\widetilde{r}_x^2)(\gamma+\widetilde{r}_y^2)(\gamma+\widetilde{r}_z^2)}}d\gamma \tag{6.1.19}$$

$$L_{r_j}\left(r_m^2\widetilde{\xi}\right) = \frac{1}{r_m^3}L^{\widetilde{r}^j}\left(\widetilde{\xi}\right) \tag{6.1.20}$$

Substituting equations (6.1.13) and (6.1.20) into equation (6.1.9):

$$G_{ij} = \delta_{ij}\left(\frac{1}{r_m^3}L^{\widetilde{r}^j}\left(\widetilde{\xi}\right) - \frac{1}{r_m^3}L^{\widetilde{r}^j}\left(\infty\right)\right) + r_m\widetilde{x}_j\left(\frac{1}{r_m^5}F^{\widetilde{r}^j}\left(\widetilde{\xi}\right)\cdot r_m\frac{\delta\widetilde{\xi}}{\delta\widetilde{x}_i}\right) \tag{6.1.21}$$

$$G_{ij} = \frac{1}{r_m^3}\left[\delta_{ij}\left(L^{\widetilde{r}^j}\left(\widetilde{\xi}\right) - L^{\widetilde{r}^j}\left(\infty\right)\right) + \widetilde{x}_j\left(F^{\widetilde{r}^j}\left(\widetilde{\xi}\right)\frac{\delta\widetilde{\xi}}{\delta\widetilde{x}_i}\right)\right] \tag{6.1.22}$$

Substituting in equation (6.1.3):

$$G_{ij} = \frac{1}{r_m^3}\widetilde{G}_{ij} \tag{6.1.23}$$

6.2 Appendix B

From equation (2.1.6):

$$\frac{\delta}{\delta x_k}G_{ij} = \frac{\delta}{\delta x_k}\left(\delta_{ij}\left(L_{r_j}(\xi) - L_{r_j}(\infty)\right) + x_j\frac{\delta L_{r_j}(\xi)}{\delta x_i}\right) \tag{6.2.1}$$

$$\frac{\delta}{\delta x_k}G_{ij} = \delta_{ij}\left(\frac{\delta L_{r_j}(\xi)}{\delta x_k} + \frac{\delta L_{r_j}(\infty)}{\delta x_k}\right) + \frac{\delta x_j}{\delta x_k}\frac{\delta L_{r_j}(\xi)}{\delta x_i} + x_j\frac{\delta}{\delta x_k}\left(\frac{\delta L_{r_j}(\xi)}{\delta x_i}\right) \tag{6.2.2}$$

$$\frac{\delta}{\delta x_k}G_{ij} = \delta_{ij}\frac{\delta L_{r_j}(\xi)}{\delta x_k} + \delta_{jk}\frac{\delta L_{r_j}(\xi)}{\delta x_i} + x_j\frac{\delta}{\delta x_k}\left(\frac{\delta L_{r_j}(\xi)}{\delta x_i}\right) \tag{6.2.3}$$

Using the chain rule, $\frac{\delta L_{r_j}(\xi)}{\delta x_i}$ is simplified to an algebraically evaluable term:

$$\frac{\delta L_{r_j}(\xi)}{\delta x_i} = \frac{\delta L_{r_j}(\xi)}{\delta \xi}\frac{\delta \xi}{\delta x_i} \tag{6.2.4}$$

$$\frac{\delta}{\delta x_k}G_{ij} = \delta_{ij}\frac{\delta L_{r_j}(\xi)}{\delta \xi}\frac{\delta \xi}{\delta x_k} + \delta_{jk}\frac{\delta L_{r_j}(\xi)}{\delta \xi}\frac{\delta \xi}{\delta x_i} + x_j\frac{\delta}{\delta x_k}\left(\frac{\delta L_{r_j}(\xi)}{\delta \xi}\frac{\delta \xi}{\delta x_i}\right) \tag{6.2.5}$$

where the derivative of ξ with respect to position equals

$$\frac{\delta \xi}{\delta x_j} = \frac{2x_j}{r_j^2+\xi}\Big/\left(\frac{x^2}{\left(r_x^2+\xi\right)^2} + \frac{y^2}{\left(r_y^2+\xi\right)^2} + \frac{z^2}{\left(r_z^2+\xi\right)^2}\right) \tag{6.2.6}$$

Using the definition of the shape parameter function given by equation (2.1.7):

$$\frac{\delta L_{r_j}(\xi)}{\delta \xi} = F_{r_j}(\xi) \tag{6.2.7}$$

$$\frac{\delta}{\delta x_k}G_{ij} = \delta_{ij}F_{r_j}(\xi)\frac{\delta \xi}{\delta x_k} + \delta_{jk}F_{r_j}(\xi)\frac{\delta \xi}{\delta x_i} + x_j\frac{\delta}{\delta x_k}\left(F_{r_j}(\xi)\frac{\delta \xi}{\delta x_i}\right) \tag{6.2.8}$$

$$\frac{\delta}{\delta x_k}G_{ij} = \delta_{ij}F_{r_j}(\xi)\frac{\delta \xi}{\delta x_k} + \delta_{jk}F_{r_j}(\xi)\frac{\delta \xi}{\delta x_i} + x_j\frac{\delta F_{r_j}(\xi)}{\delta \xi}\frac{\delta \xi}{\delta x_k}\frac{\delta \xi}{\delta x_i} + x_jF_{r_j}(\xi)\frac{\delta^2 \xi}{\delta x_i \delta x_k} \tag{6.2.9}$$

where the derivative of F_{r_j} with respect to the ellipsoidal coordinate equals

$$\begin{aligned}\frac{\delta F_{r_j}(\xi)}{\delta \xi} = &-\frac{1}{\left(\xi+\widetilde{r}_j^2\right)^2\sqrt{\left(\xi+\widetilde{r}_x^2\right)\left(\xi+\widetilde{r}_y^2\right)\left(\xi+\widetilde{r}_z^2\right)}} \\ &-\frac{\left(\xi+\widetilde{r}_x^2\right)\left(\xi+\widetilde{r}_y^2\right)+\left(\xi+\widetilde{r}_x^2\right)\left(\xi+\widetilde{r}_z^2\right)+\left(\xi+\widetilde{r}_y^2\right)\left(\xi+\widetilde{r}_z^2\right)}{2\left(\xi+\widetilde{r}_j^2\right)\left(\left(\xi+\widetilde{r}_x^2\right)\left(\xi+\widetilde{r}_y^2\right)\left(\xi+\widetilde{r}_z^2\right)\right)^{3/2}}\end{aligned} \tag{6.2.10}$$

and second derivative of the ellipsoidal coordinate with respect to position equals

$$\begin{aligned}\left[\frac{\delta^2\xi}{\delta\widetilde{x}_i\delta\widetilde{x}_k}\right]_{k=i} = &\left(\frac{2}{(\widetilde{r}_i^2+\xi)} - \frac{2\widetilde{x}_i}{(\widetilde{r}_i^2+\xi)^2}\frac{\delta\xi}{\delta\widetilde{x}_i}\right) / \left(\frac{\widetilde{x}^2}{(\widetilde{r}_x^2+\xi)^2} + \frac{\widetilde{y}^2}{(\widetilde{r}_y^2+\xi)^2} + \frac{\widetilde{z}^2}{(\widetilde{r}_z^2+\xi)^2}\right) \\ &- \frac{2\widetilde{x}_i}{(\widetilde{r}_i^2+\xi)} / \left(\frac{\widetilde{x}^2}{(\widetilde{r}_x^2+\xi)^2} + \frac{\widetilde{y}^2}{(\widetilde{r}_y^2+\xi)^2} + \frac{\widetilde{z}^2}{(\widetilde{r}_z^2+\xi)^2}\right)^2 \\ &\cdot \left(\frac{2\widetilde{x}_i}{(\widetilde{r}_i^2+\xi)^2} - \frac{\delta\xi}{\delta\widetilde{x}_i}\left(\frac{2\widetilde{x}^2}{(\widetilde{r}_x^2+\xi)^3} + \frac{2\widetilde{y}^2}{(\widetilde{r}_y^2+\xi)^3} + \frac{2\widetilde{z}^2}{(\widetilde{r}_z^2+\xi)^3}\right)\right)\end{aligned} \tag{6.2.11}$$

$$\begin{aligned}\left[\frac{\delta^2\xi}{\delta\widetilde{x}_i\delta\widetilde{x}_k}\right]_{k\neq i} = &\left(-\frac{2\widetilde{x}_i}{(\widetilde{r}_i^2+\xi)^2}\frac{\delta\xi}{\delta\widetilde{x}_k}\right)\left(\frac{\widetilde{x}^2}{(\widetilde{r}_x^2+\xi)^2} + \frac{\widetilde{y}^2}{(\widetilde{r}_y^2+\xi)^2} + \frac{\widetilde{z}^2}{(\widetilde{r}_z^2+\xi)^2}\right) \\ &- \frac{2\widetilde{x}_i}{(\widetilde{r}_i^2+\xi)}\left(\frac{\widetilde{x}^2}{(\widetilde{r}_x^2+\xi)^2} + \frac{\widetilde{y}^2}{(\widetilde{r}_y^2+\xi)^2} + \frac{\widetilde{z}^2}{(\widetilde{r}_z^2+\xi)^2}\right)^2 \\ &\cdot \left(\frac{2\widetilde{x}_k}{(\widetilde{r}_k^2+\xi)^2} - \frac{\delta\xi}{\delta\widetilde{x}_k}\left(\frac{2\widetilde{x}^2}{(\widetilde{r}_x^2+\xi)^3} + \frac{2\widetilde{y}^2}{(\widetilde{r}_y^2+\xi)^3} + \frac{2\widetilde{z}^2}{(\widetilde{r}_z^2+\xi)^3}\right)\right)\end{aligned} \tag{6.2.12}$$

6.3 Appendix C

As derived in Appendix A, the gradient of the Green tensor follows

$$\frac{\delta}{\delta x_k}G_{ij} = \delta_{ij}F_{r_j}\left(\xi\right)\frac{\delta\xi}{\delta x_k} + \delta_{jk}F_{r_j}\left(\xi\right)\frac{\delta\xi}{\delta x_i} + x_j\frac{\delta F_{r_j}\left(\xi\right)}{\delta\xi}\frac{\delta\xi}{\delta x_k}\frac{\delta\xi}{\delta x_i} + x_j F_{r_j}\left(\xi\right)\frac{\delta^2\xi}{\delta x_i\delta x_k} \tag{6.3.1}$$

In dimensionless form:

$$\frac{\delta}{\delta x_k}\widetilde{G}_{ij} = \delta_{ij}F^{\widetilde{r}^j}\left(\widetilde{\xi}\right)\frac{\delta\widetilde{\xi}}{\delta\widetilde{x}_k} + \delta_{jk}F^{\widetilde{r}^j}\left(\widetilde{\xi}\right)\frac{\delta\widetilde{\xi}}{\delta\widetilde{x}_i} + \widetilde{x}_j\frac{\delta F^{\widetilde{r}^j}\left(\widetilde{\xi}\right)}{\delta\widetilde{\xi}}\frac{\delta\widetilde{\xi}}{\delta\widetilde{x}_k}\frac{\delta\widetilde{\xi}}{\delta\widetilde{x}_i} + \widetilde{x}_j F^{\widetilde{r}^j}\left(\widetilde{\xi}\right)\frac{\delta^2\widetilde{\xi}}{\delta\widetilde{x}_i\delta\widetilde{x}_k} \tag{6.3.2}$$

Using equation (6.2.10), the dimensionless derivative of F_{r_j} with respect to ξ:

$$\begin{gathered}\frac{\delta F^{\widetilde{r}^j}\left(\widetilde{\xi}\right)}{\delta\widetilde{\xi}} = -\frac{1}{\left(\widetilde{\xi}+\widetilde{r}_j^2\right)^2\sqrt{\left(\widetilde{\xi}+\widetilde{r}_x^2\right)\left(\widetilde{\xi}+\widetilde{r}_y^2\right)\left(\widetilde{\xi}+\widetilde{r}_z^2\right)}} \\ -\frac{\left(\widetilde{\xi}+\widetilde{r}_x^2\right)\left(\widetilde{\xi}+\widetilde{r}_y^2\right)+\left(\widetilde{\xi}+\widetilde{r}_x^2\right)\left(\widetilde{\xi}+\widetilde{r}_z^2\right)+\left(\widetilde{\xi}+\widetilde{r}_y^2\right)\left(\widetilde{\xi}+\widetilde{r}_z^2\right)}{2\left(\widetilde{\xi}+\widetilde{r}_j^2\right)\left(\left(\widetilde{\xi}+\widetilde{r}_x^2\right)\left(\widetilde{\xi}+\widetilde{r}_y^2\right)\left(\widetilde{\xi}+\widetilde{r}_z^2\right)\right)^{3/2}}\end{gathered} \tag{6.3.3}$$

$$\begin{gathered}\frac{\delta F_{r_j}\left(r_m^2\widetilde{\xi}\right)}{\delta\left(r_m^2\widetilde{\xi}\right)} = -\frac{1}{\left(r_m^2\widetilde{\xi}+r_m^2\widetilde{r}_j^2\right)^2\sqrt{\left(r_m^2\widetilde{\xi}+r_m^2\widetilde{r}_x^2\right)\left(r_m^2\widetilde{\xi}+r_m^2\widetilde{r}_y^2\right)\left(r_m^2\widetilde{\xi}+r_m^2\widetilde{r}_z^2\right)}} \\ \frac{\left(r_m^2\widetilde{\xi}+r_m^2\widetilde{r}_x^2\right)\left(r_m^2\widetilde{\xi}+r_m^2\widetilde{r}_y^2\right)+\left(r_m^2\widetilde{\xi}+r_m^2\widetilde{r}_x^2\right)\left(r_m^2\widetilde{\xi}+r_m^2\widetilde{r}_z^2\right)+\left(r_m^2\widetilde{\xi}+r_m^2\widetilde{r}_y^2\right)\left(r_m^2\widetilde{\xi}+r_m^2\widetilde{r}_z^2\right)}{2\left(r_m^2\widetilde{\xi}+r_m^2\widetilde{r}_j^2\right)\left(\left(r_m^2\widetilde{\xi}+r_m^2\widetilde{r}_x^2\right)\left(r_m^2\widetilde{\xi}+r_m^2\widetilde{r}_y^2\right)\left(r_m^2\widetilde{\xi}+r_m^2\widetilde{r}_z^2\right)\right)^{3/2}}\end{gathered} \tag{6.3.4}$$

$$\begin{gathered}\frac{\delta F_{r_j}\left(r_m^2\widetilde{\xi}\right)}{\delta\left(r_m^2\widetilde{\xi}\right)} = -\frac{1}{r_m^4\left(\widetilde{\xi}+\widetilde{r}_j^2\right)^2 r_m^3\sqrt{\left(\widetilde{\xi}+\widetilde{r}_x^2\right)\left(\widetilde{\xi}+\widetilde{r}_y^2\right)\left(\widetilde{\xi}+\widetilde{r}_z^2\right)}} \\ -\frac{r_m^4\left(\left(\widetilde{\xi}+\widetilde{r}_x^2\right)\left(\widetilde{\xi}+\widetilde{r}_y^2\right)+\left(\widetilde{\xi}+\widetilde{r}_x^2\right)\left(\widetilde{\xi}+\widetilde{r}_z^2\right)+\left(\widetilde{\xi}+\widetilde{r}_y^2\right)\left(\widetilde{\xi}+\widetilde{r}_z^2\right)\right)}{2r_m^2\left(\widetilde{\xi}+\widetilde{r}_j^2\right)r_m^9\left(\left(\widetilde{\xi}+\widetilde{r}_x^2\right)\left(\widetilde{\xi}+\widetilde{r}_y^2\right)\left(\widetilde{\xi}+\widetilde{r}_z^2\right)\right)^{3/2}}\end{gathered} \tag{6.3.5}$$

$$\frac{\delta F_{r_j}\left(r_m^2\widetilde{\xi}\right)}{\delta(r_m^2\widetilde{\xi})}=\frac{1}{r_m^7}\left(-\frac{1}{\left(\widetilde{\xi}+\widetilde{r}_j^2\right)^2\sqrt{\left(\widetilde{\xi}+\widetilde{r}_x^2\right)\left(\widetilde{\xi}+\widetilde{r}_y^2\right)\left(\widetilde{\xi}+\widetilde{r}_z^2\right)}}\right.$$
$$\left.-\frac{\left(\left(\widetilde{\xi}+\widetilde{r}_x^2\right)\left(\widetilde{\xi}+\widetilde{r}_y^2\right)+\left(\widetilde{\xi}+\widetilde{r}_x^2\right)\left(\widetilde{\xi}+\widetilde{r}_z^2\right)+\left(\widetilde{\xi}+\widetilde{r}_y^2\right)\left(\widetilde{\xi}+\widetilde{r}_z^2\right)\right)}{2\left(\widetilde{\xi}+\widetilde{r}_j^2\right)\cdot\left(\left(\widetilde{\xi}+\widetilde{r}_x^2\right)\left(\widetilde{\xi}+\widetilde{r}_y^2\right)\left(\widetilde{\xi}+\widetilde{r}_z^2\right)\right)^{3/2}}\right) \tag{6.3.6}$$

$$\frac{\delta F_{r_j}\left(r_m^2\widetilde{\xi}\right)}{\delta(r_m^2\widetilde{\xi})}=\frac{1}{r_m^7}\frac{\delta F^{\widetilde{r}^j}\left(\widetilde{\xi}\right)}{\delta(\widetilde{\xi})} \tag{6.3.7}$$

The second derivative of the ellipsoidal coordinate with respect to position:

$$\frac{\delta^2\xi}{\delta x_i\delta x_k}=\frac{\delta^2\left(r_m^2\widetilde{\xi}\right)}{\delta x_i\delta x_k}=r_m^2\frac{\delta^2\widetilde{\xi}}{\delta\widetilde{x}_i\delta\widetilde{x}_k}\frac{\delta\widetilde{x}_i}{\delta x_i}\frac{\delta\widetilde{x}_k}{\delta x_k}=r_m^2\frac{\delta^2\widetilde{\xi}}{\delta\widetilde{x}_i\delta\widetilde{x}_k}\left(\frac{1}{r_m^2}\right)=\frac{\delta^2\widetilde{\xi}}{\delta\widetilde{x}_i\delta\widetilde{x}_k} \tag{6.3.8}$$

Substituting the above equations other identities from Appendix A into equation (6.3.1):

$$\frac{\delta}{\delta x_k}G_{ij}=\delta_{ij}\left(\frac{1}{r_m^5}F^{\widetilde{r}^j}\left(\widetilde{\xi}\right)\right)\left(r_m\frac{\delta\widetilde{\xi}}{\delta\widetilde{x}_k}\right)+\delta_{jk}\left(\frac{1}{r_m^5}F^{\widetilde{r}^j}\left(\widetilde{\xi}\right)\right)\left(r_m\frac{\delta\widetilde{\xi}}{\delta\widetilde{x}_i}\right)$$
$$+r_m\widetilde{x}_j\left(\frac{1}{r_m^7}\frac{\delta F^{\widetilde{r}^j}\widetilde{\xi}}{\delta(\widetilde{\xi})}\right)\left(r_m\frac{\delta\widetilde{\xi}}{\delta\widetilde{x}_k}\right)\left(r_m\frac{\delta\widetilde{\xi}}{\delta\widetilde{x}_i}\right)+r_m\widetilde{x}_j\left(\frac{1}{r_m^5}F^{\widetilde{r}^j}\left(\widetilde{\xi}\right)\right)\left(\frac{\delta^2\widetilde{\xi}}{\delta\widetilde{x}_i\delta\widetilde{x}_k}\right) \tag{6.3.9}$$

$$\frac{\delta}{\delta x_k}G_{ij}=\frac{1}{r_m^4}\left(\delta_{ij}F^{\widetilde{r}^j}\left(\widetilde{\xi}\right)\frac{\delta\widetilde{\xi}}{\delta\widetilde{x}_k}+\delta_{jk}F^{\widetilde{r}^j}\left(\widetilde{\xi}\right)\frac{\delta\widetilde{\xi}}{\delta\widetilde{x}_i}+\widetilde{x}_j\frac{\delta F^{\widetilde{r}^j}\left(\widetilde{\xi}\right)}{\delta\widetilde{\xi}}\frac{\delta\widetilde{\xi}}{\delta\widetilde{x}_k}\frac{\delta\widetilde{\xi}}{\delta\widetilde{x}_i}+\widetilde{x}_jF^{\widetilde{r}^j}\left(\widetilde{\xi}\right)\frac{\delta^2\widetilde{\xi}}{\delta\widetilde{x}_i\delta\widetilde{x}_k}\right) \tag{6.3.10}$$

Substituting in equation (6.3.2):

$$\frac{\delta}{\delta x_k}G_{ij}=\frac{1}{r_m^4}\frac{\delta}{\delta x_k}\widetilde{G}_{ij} \tag{6.3.11}$$

6.4 Appendix D

According to Evans [12]:

$$\omega^{(2)} = \frac{\delta \mathbf{A}}{\delta t}\mathbf{A}^T \tag{6.4.1}$$

where $\omega^{(2)} = \epsilon \cdot \omega$ is the skew-symmetric tensor form of the angular velocity vector $\omega = \delta\mathbf{\Phi}/\delta t$, and ϵ is the Levi-Civita tensor. Using these identities in equation (6.4.1) gives

$$\epsilon \cdot \frac{\delta \mathbf{\Phi}}{\delta t} = \frac{\delta \mathbf{A}}{\delta t}\mathbf{A}^T \tag{6.4.2}$$

Using the chain rule:

$$\epsilon \cdot \frac{\delta \mathbf{\Phi}}{\delta \mathbf{q}}\frac{\delta \mathbf{q}}{\delta t} = \frac{\delta \mathbf{A}}{\delta t}\mathbf{A}^T \tag{6.4.3}$$

For a quaternion defined by equation (1.2.2) and the associated transformation matrix as defined by equation (1.2.8):

$$\frac{\delta \mathbf{A}}{\delta t} = \dot{\mathbf{A}} = \begin{bmatrix} 2(q_0\dot{q_0} + q_1\dot{q_1} - q_2\dot{q_2} - q_3\dot{q_3}) & 2(q_1\dot{q_2} + \dot{q_1}q_2 - q_0\dot{q_3} - \dot{q_0}q_3) & 2(q_1\dot{q_3} + \dot{q_1}q_3 + q_0\dot{q_2} + \dot{q_0}q_2) \\ 2(q_1\dot{q_2} + \dot{q_1}q_2 + q_0\dot{q_3} + \dot{q_0}q_3) & 2(q_0\dot{q_0} - q_1\dot{q_1} + q_2\dot{q_2} - q_3\dot{q_3}) & 2(q_3\dot{q_2} + \dot{q_3}q_2 - q_0\dot{q_1} - \dot{q_0}q_1) \\ 2(q_1\dot{q_3} + \dot{q_1}q_3 - q_0\dot{q_2} - \dot{q_0}q_2) & 2(q_3\dot{q_2} + \dot{q_3}q_2 + q_0\dot{q_1} + \dot{q_0}q_1) & 2(q_0\dot{q_0} - q_1\dot{q_1} - q_2\dot{q_2} + q_3\dot{q_3}) \end{bmatrix} \tag{6.4.4}$$

$$\mathbf{A}^T = \begin{bmatrix} q_0^2 + q_1^2 - q_2^2 - q_3^2 & 2(q_2q_1 + q_0q_3) & 2(q_3q_1 - q_0q_2) \\ 2(q_1q_2 - q_0q_3) & q_0^2 - q_1^2 + q_2^2 - q_3^2 & 2(q_3q_2 + q_0q_1) \\ 2(q_1q_3 + q_0q_2) & 2(q_2q_3 - q_0q_1) & q_0^2 - q_1^2 - q_2^2 + q_3^2 \end{bmatrix} \tag{6.4.5}$$

Substituting these expressions into equation (6.4.3), multiplying the matrices, and using the properties of unit quaternions (namely, $q_0^2 + q_1^2 + q_2^2 + q_3^2 = 1$ and $q_0\dot{q_0} + q_1\dot{q_1} + q_2\dot{q_2} + q_3\dot{q_3} = 0$) to reduce the result yields

$$\epsilon \cdot \frac{\delta \mathbf{\Phi}}{\delta \mathbf{q}}\frac{\delta \mathbf{q}}{\delta t} = \begin{bmatrix} 0 & 2(q_3\dot{q_0} + q_2\dot{q_1} - q_1\dot{q_2} - q_0\dot{q_3}) & -2(q_2\dot{q_0} - q_3\dot{q_1} - q_0\dot{q_2} + q_1\dot{q_3}) \\ -2(q_3\dot{q_0} + q_2\dot{q_1} - q_1\dot{q_2} - q_0\dot{q_3}) & 0 & 2(q_1\dot{q_0} - q_0\dot{q_1} + q_3\dot{q_2} - q_2\dot{q_3}) \\ 2(q_2\dot{q_0} - q_3\dot{q_1} - q_0\dot{q_2} + q_1\dot{q_3}) & -2(q_1\dot{q_0} - q_0\dot{q_1} + q_3\dot{q_2} - q_2\dot{q_3}) & 0 \end{bmatrix} \tag{6.4.6}$$

As expected, the matrix in equation (6.4.7) is skew-symmetric. Thus, using the properties of the Levi-Civita tensor, the equation can be solved in reverse to to isolate $\delta\mathbf{\Phi}/\delta\mathbf{q}$:

$$\frac{\delta \mathbf{\Phi}}{\delta \mathbf{q}}\frac{\delta \mathbf{q}}{\delta t} = 2\begin{bmatrix} q_1\dot{q_0} - q_0\dot{q_1} + q_3\dot{q_2} - q_2\dot{q_3} \\ q_2\dot{q_0} - q_3\dot{q_1} - q_0\dot{q_2} + q_1\dot{q_3} \\ q_3\dot{q_0} + q_2\dot{q_1} - q_1\dot{q_2} - q_0\dot{q_3} \end{bmatrix} \tag{6.4.7}$$

$$\frac{\delta \mathbf{\Phi}}{\delta \mathbf{q}} = 2\begin{bmatrix} q_1\dot{q_0} - q_0\dot{q_1} + q_3\dot{q_2} - q_2\dot{q_3} \\ q_2\dot{q_0} - q_3\dot{q_1} - q_0\dot{q_2} + q_1\dot{q_3} \\ q_3\dot{q_0} + q_2\dot{q_1} - q_1\dot{q_2} - q_0\dot{q_3} \end{bmatrix}\frac{\delta t}{\delta \mathbf{q}} \tag{6.4.8}$$

Factoring out the time derivative of the quaternion reduces the above relation as follows:

$$\frac{\delta \mathbf{\Phi}}{\delta \mathbf{q}} = 2\begin{bmatrix} q_1 & -q_0 & q_3 & -q_2 \\ q_2 & -q_3 & -q_0 & q_1 \\ q_3 & q_2 & -q_1 & -q_0 \end{bmatrix}\frac{\delta \mathbf{q}}{\delta t}\frac{\delta t}{\delta \mathbf{q}} \tag{6.4.9}$$

$$\frac{\delta \mathbf{\Phi}}{\delta \mathbf{q}} = 2 \begin{bmatrix} q_1 & -q_0 & q_3 & -q_2 \\ q_2 & -q_3 & -q_0 & q_1 \\ q_3 & q_2 & -q_1 & -q_0 \end{bmatrix} \tag{6.4.10}$$

As defined by Delong [14]:

$$\mathbf{\Psi} = \frac{\delta \mathbf{q}}{\delta \mathbf{\Phi}} \tag{6.4.11}$$

Relating this definition to the matrix defined in equation (6.4.10):

$$\mathbf{\Psi} \frac{\delta \mathbf{\Phi}}{\delta \mathbf{q}} = \frac{\delta \mathbf{q}}{\delta \mathbf{\Phi}} \frac{\delta \mathbf{\Phi}}{\delta \mathbf{q}} = \mathbf{I} \tag{6.4.12}$$

where $\mathbf{I}$ is the identity matrix. In matrix form:

$$\mathbf{\Psi} \cdot 2 \begin{bmatrix} q_1 & -q_0 & q_3 & -q_2 \\ q_2 & -q_3 & -q_0 & q_1 \\ q_3 & q_2 & -q_1 & -q_0 \end{bmatrix} = \mathbf{I} \tag{6.4.13}$$

Solving for $\mathbf{\Psi}$:

$$\mathbf{\Psi} = \frac{1}{2} \begin{bmatrix} q_1 & q_2 & q_3 \\ -q_0 & -q_3 & q_2 \\ q_3 & -q_0 & -q_1 \\ -q_2 & q_1 & -q_0 \end{bmatrix} \tag{6.4.14}$$

6.5 Appendix E

According to equation (3.3.5), the translational mobility matrix equals

$$\mathbf{K} = 16\pi\mu \left[\frac{1}{X + {r_x}^2 L^{r^x}(\infty)} \mathbf{e_x e_x} + \frac{1}{{r_y}^2 L^{r^y}(\infty)} \mathbf{e_y e_y} + \frac{1}{{r_z}^2 L^{r^z}(\infty)} \mathbf{e_z e_z} \right] \tag{6.5.1}$$

Defining the dimensionless form as

$$\widetilde{\mathbf{K}} = \left[\frac{1}{\widetilde{X} + \widetilde{r}_x^2 L^{\widetilde{r}^x}(\infty)} \mathbf{e_x e_x} + \frac{1}{\widetilde{X} + \widetilde{r}_y^2 L^{\widetilde{r}^y}(\infty)} \mathbf{e_y e_y} + \frac{1}{\widetilde{X} + \widetilde{r}_z^2 L^{\widetilde{r}^z}(\infty)} \mathbf{e_z e_z} \right] \tag{6.5.2}$$

According to equation (6.1.20):

$$L_i(\infty) = \frac{1}{r_m^3} \widetilde{L}^i(\infty) \tag{6.5.3}$$

The dimensionless form of the X function:

$$\widetilde{X} = \int_0^\infty \frac{1}{\sqrt{\left(\alpha + \widetilde{r}_x^2\right)\left(\alpha + \widetilde{r}_y^2\right)\left(\alpha + \widetilde{r}_z^2\right)}} d\alpha \tag{6.5.4}$$

$$X = \int_0^\infty \frac{1}{\sqrt{\left(\alpha + r_m^2 \widetilde{r}_x^2\right)\left(\alpha + r_m^2 \widetilde{r}_y^2\right)\left(\alpha + r_m^2 \widetilde{r}_z^2\right)}} d\alpha \tag{6.5.5}$$

$$\gamma = \frac{\alpha}{r_m^2} \ , \quad d\gamma = \frac{d\alpha}{r_m^2} \tag{6.5.6}$$

$$X = \int_0^{\infty/r_m^2} \frac{r_m^2}{\sqrt{\left(r_m^2\gamma + r_m^2 \widetilde{r}_x^2\right)\left(r_m^2\gamma + r_m^2 \widetilde{r}_y^2\right)\left(r_m^2\gamma + r_m^2 \widetilde{r}_z^2\right)}} d\gamma \tag{6.5.7}$$

$$X = \frac{1}{r_m} \int_0^\infty \frac{1}{\sqrt{\left(\gamma + \widetilde{r}_x^2\right)\left(\gamma + \widetilde{r}_y^2\right)\left(\gamma + \widetilde{r}_z^2\right)}} d\gamma \tag{6.5.8}$$

$$X = \frac{1}{r_m} \widetilde{X} \tag{6.5.9}$$

Substituting these values into equation (6.5.1):

$$\begin{aligned} \mathbf{K} = 16\pi\mu \Bigg[& \frac{1}{\frac{1}{r_m}\widetilde{X} + r_m^2 \widetilde{r}_x^2 \left(\frac{1}{r_m^3} L^{\widetilde{r}^x}(\infty) \right)} \mathbf{e_x e_x} + \frac{1}{\frac{1}{r_m}\widetilde{X} + r_m^2 \widetilde{r_y}^2 \left(\frac{1}{r_m^3} L^{\widetilde{r}^y}(\infty) \right)} \mathbf{e_y e_y} \\ & + \frac{1}{\frac{1}{r_m}\widetilde{X} + r_m^2 \widetilde{r_z}^2 \left(\frac{1}{r_m^3} L^{\widetilde{r}^z}(\infty) \right)} \mathbf{e_z e_z} \Bigg] \end{aligned} \tag{6.5.10}$$

$$\mathbf{K} = 16\pi\mu r_m \left[\frac{1}{\widetilde{X} + \widetilde{r}_x^2 L^{\widetilde{r}^x}(\infty)} \mathbf{e_x e_x} + \frac{1}{\widetilde{X} + \widetilde{r_y}^2 L^{\widetilde{r}^y}(\infty)} \mathbf{e_y e_y} + \frac{1}{\widetilde{X} + \widetilde{r_z}^2 L^{\widetilde{r}^z}(\infty)} \mathbf{e_z e_z} \right] \tag{6.5.11}$$

$$\mathbf{K} = 16\pi\mu r_m \widetilde{\mathbf{K}} \tag{6.5.12}$$

According to equation (3.3.6), the rotational mobility matrix equals

$$\mathbf{\Omega} = \frac{16\pi}{3}\mu \left[\frac{{r_y}^2+{r_z}^2}{{r_y}^2 L^{r^x}(\infty)+{r_z}^2 L^{r^x}(\infty)}\mathbf{e_x}\mathbf{e_x} + \frac{{r_x}^2+{r_z}^2}{{r_x}^2 L^{r^y}(\infty)+{r_z}^2 L^{r^y}(\infty)}\mathbf{e_y}\mathbf{e_y} + \frac{{r_x}^2+{r_y}^2}{{r_x}^2 L^{r^z}(\infty)+{r_y}^2 L^{r^z}(\infty)}\mathbf{e_z}\mathbf{e_z} \right] \tag{6.5.13}$$

Defining dimensionless form as

$$\widetilde{\mathbf{\Omega}} = \left[\frac{\widetilde{r}_y^2+\widetilde{r}_z^2}{\widetilde{r}_y^2 L^{\widetilde{r}^x}(\infty)+\widetilde{r}_z^2 L^{\widetilde{r}^x}(\infty)}\mathbf{e_x}\mathbf{e_x} + \frac{\widetilde{r}_x^2+\widetilde{r}_z^2}{\widetilde{r}_x^2 L^{\widetilde{r}^y}(\infty)+\widetilde{r}_z^2 L^{\widetilde{r}^y}(\infty)}\mathbf{e_y}\mathbf{e_y} + \frac{\widetilde{r}_x^2+\widetilde{r}_y^2}{\widetilde{r}_x^2 L^{\widetilde{r}^z}(\infty)+\widetilde{r}_y^2 L^{\widetilde{r}^z}(\infty)}\mathbf{e_z}\mathbf{e_z} \right] \tag{6.5.14}$$

Using the definitions of dimensionless variables derived in Appendix A:

$$\begin{aligned} \mathbf{\Omega} = \frac{16\pi}{3}\mu \Bigg[& \frac{r_m^2\widetilde{r}_y^2 + r_m^2\widetilde{r}_z^2}{r_m^2\widetilde{r}_y^2\left(\frac{1}{r_m^3}L^{\widetilde{r}^x}(\infty)\right) + r_m^2\widetilde{r}_z^2\left(\frac{1}{r_m^3}L^{\widetilde{r}^x}(\infty)\right)}\mathbf{e_x}\mathbf{e_x} \\ & + \frac{r_m^2\widetilde{r}_x^2 + r_m^2\widetilde{r}_z^2}{r_m^2\widetilde{r}_x^2\left(\frac{1}{r_m^3}L^{\widetilde{r}^y}(\infty)\right) + r_m^2\widetilde{r}_z^2\left(\frac{1}{r_m^3}L^{\widetilde{r}^y}(\infty)\right)}\mathbf{e_y}\mathbf{e_y} \\ & + \frac{r_m^2\widetilde{r}_x^2 + r_m^2\widetilde{r}_y^2}{r_m^2\widetilde{r}_x^2\left(\frac{1}{r_m^3}L^{\widetilde{r}^z}(\infty)\right) + r_m^2\widetilde{r}_y^2\left(\frac{1}{r_m^3}L^{\widetilde{r}^z}(\infty)\right)}\mathbf{e_z}\mathbf{e_z} \Bigg] \end{aligned} \tag{6.5.15}$$

$$\begin{aligned} \widetilde{\mathbf{\Omega}} = \frac{16\pi}{3}\mu r_m^3 \Bigg[& \frac{\widetilde{r}_y^2 + \widetilde{r}_z^2}{\widetilde{r}_y^2 L^{\widetilde{r}^x}(\infty) + \widetilde{r}_z^2 L^{\widetilde{r}^x}(\infty)}\mathbf{e_x}\mathbf{e_x} + \frac{\widetilde{r}_x^2 + \widetilde{r}_z^2}{\widetilde{r}_x^2 L^{\widetilde{r}^y}(\infty) + \widetilde{r}_z^2 L^{\widetilde{r}^y}(\infty)}\mathbf{e_y}\mathbf{e_y} \\ & + \frac{\widetilde{r}_x^2 + \widetilde{r}_y^2}{\widetilde{r}_x^2 L^{\widetilde{r}^z}(\infty) + \widetilde{r}_y^2 L^{\widetilde{r}^z}(\infty)}\mathbf{e_z}\mathbf{e_z} \Bigg] \end{aligned} \tag{6.5.16}$$

$$\mathbf{\Omega} = \frac{16\pi}{3}\mu r_m^3 \widetilde{\mathbf{\Omega}} \tag{6.5.17}$$

6.6 Appendix F

According to equation (3.3.12), the Lagrange Equation in terms of the grand resistance matrix and the diffusivity tensors equals

$$\begin{pmatrix}\Delta\mathbf{x}\\ \Delta\mathbf{\Phi}\end{pmatrix} = \Delta t\mathcal{M}\begin{pmatrix}\mathbf{F}_{dd}\\ \tau_{dd}\end{pmatrix} + \Delta t\mathcal{M}\begin{pmatrix}\mathbf{F}_{df}\\ \tau_{df}\end{pmatrix} + \Delta t\mathcal{M}\begin{pmatrix}\mathbf{F}_{e}\\ \tau_{e}\end{pmatrix} - \begin{pmatrix}\sqrt{2\mathbf{D}_x\Delta t}(BM)\\ \sqrt{2\mathbf{D}_r\Delta t}(BM)\end{pmatrix}. \tag{6.6.1}$$

Substituting in the definitions of $\mathcal{M}$, $\mathbf{D_x}$, and $\mathbf{D_x}$ yields

$$\begin{aligned}\begin{pmatrix}\Delta\mathbf{x}\\ \Delta\mathbf{\Phi}\end{pmatrix} = \Delta t\begin{pmatrix}\mathbf{K}^{-1} & 0\\ 0 & \mathbf{\Omega}^{-1}\end{pmatrix}\begin{pmatrix}\mathbf{F}_{dd}\\ \tau_{dd}\end{pmatrix} + \Delta t\begin{pmatrix}\mathbf{K}^{-1} & 0\\ 0 & \mathbf{\Omega}^{-1}\end{pmatrix}\begin{pmatrix}\mathbf{F}_{dd}\\ \tau_{dd}\end{pmatrix}\\ +\Delta t\begin{pmatrix}\mathbf{K}^{-1} & 0\\ 0 & \mathbf{\Omega}^{-1}\end{pmatrix}\begin{pmatrix}\mathbf{F}_{dd}\\ \tau_{dd}\end{pmatrix} - \begin{pmatrix}\sqrt{2k_BT\mathbf{K}^{-1}\Delta t}(BM)\\ \sqrt{2k_BT\mathbf{\Omega}^{-1}\Delta t}(BM)\end{pmatrix},\end{aligned} \tag{6.6.2}$$

Using dimensionless variables results in

$$\begin{aligned}\begin{pmatrix}r_m\Delta\widetilde{\mathbf{x}}\\ \Delta\mathbf{\Phi}\end{pmatrix} = \frac{\Delta\widetilde{t}}{D_{r,max}}\begin{pmatrix}\mathbf{K}^{-1} & 0\\ 0 & \mathbf{\Omega}^{-1}\end{pmatrix}\begin{pmatrix}k_BTr_m^{-1}\widetilde{\mathbf{F}}_{dd}\\ k_BT\widetilde{\tau}_{dd}\end{pmatrix}\\ +\frac{\Delta\widetilde{t}}{D_{r,max}}\begin{pmatrix}\mathbf{K}^{-1} & 0\\ 0 & \mathbf{\Omega}^{-1}\end{pmatrix}\begin{pmatrix}k_BTr_m^{-1}\widetilde{\mathbf{F}}_{df}\\ k_BT\widetilde{\tau}_{df}\end{pmatrix}\\ +\frac{\Delta\widetilde{t}}{D_{r,max}}\begin{pmatrix}\mathbf{K}^{-1} & 0\\ 0 & \mathbf{\Omega}^{-1}\end{pmatrix}\begin{pmatrix}k_BTr_m^{-1}\widetilde{\mathbf{F}}_{e}\\ k_BT\widetilde{\tau}_{e}\end{pmatrix}\\ -\begin{pmatrix}\sqrt{2k_BT\mathbf{K}^{-1}\Delta\widetilde{t}D_{r,max}^{-1}}(BM)\\ \sqrt{2k_BT\mathbf{\Omega}^{-1}\Delta\widetilde{t}D_{r,max}^{-1}}(BM)\end{pmatrix},\end{aligned} \tag{6.6.3}$$

Further utilizing the definitions of $\mathbf{D_x}$ and $\mathbf{D_x}$ yields

$$\begin{aligned}\begin{pmatrix}r_m\Delta\widetilde{\mathbf{x}}\\ \Delta\mathbf{\Phi}\end{pmatrix} = \Delta\widetilde{t}\frac{\Omega_{min}}{k_BT}\begin{pmatrix}\mathbf{K}^{-1} & 0\\ 0 & \mathbf{\Omega}^{-1}\end{pmatrix}\begin{pmatrix}k_BTr_m^{-1}\widetilde{\mathbf{F}}_{dd}\\ k_BT\widetilde{\tau}_{dd}\end{pmatrix}\\ +\Delta\widetilde{t}\frac{\Omega_{min}}{k_BT}\begin{pmatrix}\mathbf{K}^{-1} & 0\\ 0 & \mathbf{\Omega}^{-1}\end{pmatrix}\begin{pmatrix}k_BTr_m^{-1}\widetilde{\mathbf{F}}_{df}\\ k_BT\widetilde{\tau}_{df}\end{pmatrix}\\ +\Delta\widetilde{t}\frac{\Omega_{min}}{k_BT}\begin{pmatrix}\mathbf{K}^{-1} & 0\\ 0 & \mathbf{\Omega}^{-1}\end{pmatrix}\begin{pmatrix}k_BTr_m^{-1}\widetilde{\mathbf{F}}_{e}\\ k_BT\widetilde{\tau}_{e}\end{pmatrix}\\ -\begin{pmatrix}\sqrt{2k_BT\mathbf{K}^{-1}\Delta\widetilde{t}\frac{\Omega_{min}}{k_BT}}(BM)\\ \sqrt{2k_BT\mathbf{\Omega}^{-1}\Delta\widetilde{t}\frac{\Omega_{min}}{k_BT}}(BM)\end{pmatrix},\end{aligned} \tag{6.6.4}$$

where Ω_{min} is the minimum diagonal component of $\mathbf{\Omega}$ among all particles in the simulation. Applying the dimensionless forms of the resistance dyadics and simplifying gives

$$\begin{aligned}\begin{pmatrix}\Delta\widetilde{\mathbf{x}}\\ \Delta\mathbf{\Phi}\end{pmatrix} &= \Delta\widetilde{t}\frac{16\pi}{3}\mu r_m^3\widetilde{\Omega}_{min}\begin{pmatrix}\frac{\widetilde{\mathbf{K}}^{-1}}{16\pi\mu r_m} & 0\\ 0 & \frac{3\widetilde{\mathbf{\Omega}}^{-1}}{16\pi\mu r_m^3}\end{pmatrix}\begin{pmatrix}r_m^{-2}\widetilde{\mathbf{F}}_{dd}\\ \widetilde{\tau}_{dd}\end{pmatrix}\\ &+\Delta\widetilde{t}\frac{16\pi}{3}\mu r_m^3\widetilde{\Omega}_{min}\begin{pmatrix}\frac{\widetilde{\mathbf{K}}^{-1}}{16\pi\mu r_m} & 0\\ 0 & \frac{3\widetilde{\mathbf{\Omega}}^{-1}}{16\pi\mu r_m^3}\end{pmatrix}\begin{pmatrix}r_m^{-2}\widetilde{\mathbf{F}}_{df}\\ \widetilde{\tau}_{df}\end{pmatrix}\\ &+\Delta\widetilde{t}\frac{16\pi}{3}\mu r_m^3\widetilde{\Omega}_{min}\begin{pmatrix}\frac{\widetilde{\mathbf{K}}^{-1}}{16\pi\mu r_m} & 0\\ 0 & \frac{3\widetilde{\mathbf{\Omega}}^{-1}}{16\pi\mu r_m^3}\end{pmatrix}\begin{pmatrix}r_m^{-2}\widetilde{\mathbf{F}}_{e}\\ \widetilde{\tau}_{e}\end{pmatrix}\\ &-\begin{pmatrix}r_m^{-1}\sqrt{2\frac{\widetilde{\mathbf{K}}^{-1}}{16\pi\mu r_m}\Delta\widetilde{t}\frac{16}{3}\pi\mu r_m^3\widetilde{\Omega}_{min}}(BM)\\ \sqrt{2\frac{3\widetilde{\mathbf{\Omega}}^{-1}}{16\pi\mu r_m^3}\Delta\widetilde{t}\frac{16}{3}\pi\mu r_m^3\widetilde{\Omega}_{min}}(BM)\end{pmatrix},\end{aligned} \tag{6.6.5}$$

$$\begin{aligned}\begin{pmatrix}\Delta\widetilde{\mathbf{x}}\\ \Delta\mathbf{\Phi}\end{pmatrix} &= \Delta\widetilde{t}\widetilde{\Omega}_{min}\begin{pmatrix}\frac{1}{3}\widetilde{\mathbf{K}}^{-1} & 0\\ 0 & \widetilde{\mathbf{\Omega}}^{-1}\end{pmatrix}\begin{pmatrix}\widetilde{\mathbf{F}}_{dd}\\ \widetilde{\tau}_{dd}\end{pmatrix}\\ &+\Delta\widetilde{t}\widetilde{\Omega}_{min}\begin{pmatrix}\frac{1}{3}\widetilde{\mathbf{K}}^{-1} & 0\\ 0 & \widetilde{\mathbf{\Omega}}^{-1}\end{pmatrix}\begin{pmatrix}\widetilde{\mathbf{F}}_{df}\\ \widetilde{\tau}_{df}\end{pmatrix}\\ &+\Delta\widetilde{t}\widetilde{\Omega}_{min}\begin{pmatrix}\frac{1}{3}\widetilde{\mathbf{K}}^{-1} & 0\\ 0 & \widetilde{\mathbf{\Omega}}^{-1}\end{pmatrix}\begin{pmatrix}\widetilde{\mathbf{F}}_{e}\\ \widetilde{\tau}_{e}\end{pmatrix}\\ &-\begin{pmatrix}\sqrt{\frac{2}{3}\widetilde{\mathbf{K}}^{-1}\Delta\widetilde{t}\widetilde{\Omega}_{min}}(BM)\\ \sqrt{2\widetilde{\mathbf{\Omega}}^{-1}\Delta\widetilde{t}\widetilde{\Omega}_{min}}(BM)\end{pmatrix},\end{aligned} \tag{6.6.6}$$

To condense this expression, this dimensionless mobility matrix $\widetilde{\mathcal{M}}$ is defined according to equation (3.3.18), which yields

$$\begin{pmatrix}\Delta\widetilde{\mathbf{x}}\\ \Delta\mathbf{\Phi}\end{pmatrix} = \Delta\widetilde{t}\widetilde{\mathcal{M}}\begin{pmatrix}\widetilde{\mathbf{F}}_{dd}\\ \widetilde{\tau}_{dd}\end{pmatrix} + \Delta\widetilde{t}\widetilde{\mathcal{M}}\begin{pmatrix}\widetilde{\mathbf{F}}_{df}\\ \widetilde{\tau}_{df}\end{pmatrix} + \Delta\widetilde{t}\widetilde{\mathcal{M}}\begin{pmatrix}\widetilde{\mathbf{F}}_{e}\\ \widetilde{\tau}_{e}\end{pmatrix} - \begin{pmatrix}\sqrt{\frac{2}{3}\Delta\widetilde{t}\widetilde{\Omega}_{min}\widetilde{\mathbf{K}}^{-1}}(BM)\\ \sqrt{2\Delta\widetilde{t}\widetilde{\Omega}_{min}\widetilde{\mathbf{\Omega}}^{-1}}(BM)\end{pmatrix}, \tag{6.6.7}$$

Because this report uses quaternions to track orientation, the change in orientation is transformed to a change in quaternion using $\mathbf{\Psi}$ according to

$$\begin{pmatrix}\Delta\widetilde{\mathbf{x}}\\ \frac{\delta\mathbf{\Phi}}{\delta\mathbf{q}}\Delta\mathbf{q}\end{pmatrix} = \Delta\widetilde{t}\widetilde{\mathcal{M}}\begin{pmatrix}\widetilde{\mathbf{F}}_{dd}\\ \widetilde{\tau}_{dd}\end{pmatrix} + \Delta\widetilde{t}\widetilde{\mathcal{M}}\begin{pmatrix}\widetilde{\mathbf{F}}_{df}\\ \widetilde{\tau}_{df}\end{pmatrix} + \Delta\widetilde{t}\widetilde{\mathcal{M}}\begin{pmatrix}\widetilde{\mathbf{F}}_{e}\\ \widetilde{\tau}_{e}\end{pmatrix} - \begin{pmatrix}\sqrt{\frac{2}{3}\Delta\widetilde{t}\widetilde{\Omega}_{min}\widetilde{\mathbf{K}}^{-1}}(BM)\\ \sqrt{2\Delta\widetilde{t}\widetilde{\Omega}_{min}\widetilde{\mathbf{\Omega}}^{-1}}(BM)\end{pmatrix}, \tag{6.6.8}$$

$$\begin{pmatrix}\Delta\widetilde{\mathbf{x}}\\ \Delta\mathbf{q}\end{pmatrix} = \begin{pmatrix}\mathbf{I}\\ \mathbf{\Psi}\end{pmatrix}\left[\Delta\widetilde{t}\widetilde{\mathcal{M}}\begin{pmatrix}\widetilde{\mathbf{F}}_{dd}\\ \widetilde{\tau}_{dd}\end{pmatrix} + \Delta\widetilde{t}\widetilde{\mathcal{M}}\begin{pmatrix}\widetilde{\mathbf{F}}_{df}\\ \widetilde{\tau}_{df}\end{pmatrix} + \Delta\widetilde{t}\widetilde{\mathcal{M}}\begin{pmatrix}\widetilde{\mathbf{F}}_{e}\\ \widetilde{\tau}_{e}\end{pmatrix} - \begin{pmatrix}\sqrt{\frac{2}{3}\Delta\widetilde{t}\widetilde{\Omega}_{min}\widetilde{\mathbf{K}}^{-1}}(BM)\\ \sqrt{2\Delta\widetilde{t}\widetilde{\Omega}_{min}\widetilde{\mathbf{\Omega}}^{-1}}(BM)\end{pmatrix}\right], \tag{6.6.9}$$